Materials Advances

ROYAL SOCIETY OF CHEMISTRY

PAPER

View Article Online
View Journal | View Issue

Open Access Article. Published on 19 August 2025. Downloaded on 3/29/2026 11:26:00 PM.
This article is licensed under a Creative Commons Attribution-NonCommercial 3.0 Unported Licence.

Check for updates

Cite this: *Mater. Adv.*, 2025, **6**, 6991

Synthesis of novel azo dye-based 1,2,4-triazine derivatives and their spectral, fabric and anti-bacterial applications: an integration of solvatochromism, photochromism, colorfastness, TD-DFT and molecular docking analysis

Saima Aslam,[a] Basharat Ali,*[a] Shahzad Murtaza[a] and Nusrat Shafiq *[b]

Received 4th June 2025,
Accepted 18th August 2025

DOI: 10.1039/d5ma00587f

rsc.li/materials-advances

In the current research, a series of five novel azo dyes (**1c–5c**) were synthesized from azodiene (**1a–5a**) and azodienophile (**1b–5b**) *via* the Diels–Alder reaction. These 1,2,4-triazine derivatives (**1c–5c**) were synthesized through grindstone synthesis and characterized through ^{13}C-NMR and ^{1}H-NMR. Further, they were evaluated for their dye potential by textile application using an ISO-certified method. The colorfastness properties of these dyes were checked by ISO standard methods on polyester fabric. These were screened for their *in vitro* antibacterial activities against Gram-negative and Gram-positive bacteria at 50, 100, 150, 200 and 250 mg mL^{-1} concentrations using cephalosporin as the standard drug. The synthesized dyes/compounds revealed good results against *E. coli* and *Staphylococcus aureus* strains. Moreover, molecular docking of these dyes was done by Molegro Virtual Docker with very good MolDock scores. Solvatochromism of these dyes was checked based on their λ_{max} values, and their photochromism was also checked by applying sunlight to their solvent solutions. These values were compared with experimental and TD-SCF DFT values, showing almost the same results.

1. Introduction

The textile industry (wool, polyamides and cotton) uses dyes on a large scale due to their different color shades, applications, eminent wet fastness and radiant colors.[1,2] Without using any chemical process, vegetable- and animal matter-based dyes are natural dyes. Another type is synthetic dyes, which are more advantageous than natural dyes due to their color fastness, color shade, availability and applications.[3] Among them, azo dyes are the major class of synthetic dyes.[4] Depending on their solubility, dyes are grouped into reactive (water soluble) and disperse dyes (water insoluble).[5–7] Azo dyes are chromophores that can be used to color synthetic and natural fibers.[8] In industry, about 70% of dyes are azo dyes. They are mainly used in the paint, textile, food, cosmetics, paper, pharmaceutical and leather industries.[9]

Azo dyes are preferred due to their coupling reaction, structure variation and accommodation to the requirement[10] with the additional feature of having various shades of different color intensities of the same dye due to the substituent on their side aromatic groups.[11] These dyes are synthesized within a short reaction time and under moderate reaction conditions. They also require less energy consumption and produce good yields.[4] Their color strength and dye fixation can be enhanced by optimizing the dye conditions. Various factors such as the nature of the fabric, reaction time, chemical auxiliaries, pH of the medium, dyeing temperature, nature of dye and dyeing procedure affect the color strength and dye fixation. By controlling these factors, the dye discharge in wastewater can be reduced to ensure a sustainable environment. In addition to functional group number, its position in the dye structure plays a key role in controlling dye fixation.[12]

Azo dye derivatives exhibit pharmaceutical activities, including antimicrobial,[13–15] anti-tumor,[16–18] antioxidant,[19,20] and anti-inflammatory activities,[21–23] and are also used in non-linear optics, lasers, plastics, thermal transfer printers, metallochromic indicators, fuel cells, paper, leather, cosmetics, food and photodynamic therapy.[7] Moreover, 1,2,4-triazine plays a vital role in dye-sensitized solar cells.[24] Triazine derivatives have fundamental applications such as optical bleaches, textiles, surface active agents, plastics, rubber production and pharmaceuticals. They are extensively used in thermally active delayed

[a] *Institute of Chemistry, Khwaja Fareed University of Engineering & Information Technology, Rahim Yar Khan, Pakistan. E-mail: saimaaslam565@gmail.com, basharat.ali@kfueit.edu.pk, Shahzad.murtaza@kfueit.edu.pk*

[b] *Synthetic and Natural Products Discovery (SNPD) Laboratory, Department of Chemistry, Government College Women University, Faisalabad-38000, Pakistan. E-mail: dr.nusratshafiq@gcwuf.edu.pk, gqumarin@gmail.com*

© 2025 The Author(s). Published by the Royal Society of Chemistry

Open Access Article. Published on 19 August 2025. Downloaded on 3/29/2026 11:26:00 PM.
This article is licensed under a Creative Commons Attribution-NonCommercial 3.0 Unported Licence.

fluorescence emitters, organic light-emitting diodes as electron transport materials and in bulk heterojunction solar cells as donors. They have great ability with metal ions to form complexes.[25] On account of economic and environmental reasons, disperse dyes are well-known and considered as a significant class for dyeing polyester fibers owing to their excellent fastness features.[26]

In the current study, five disperse dyes, namely 1,2,4-triazine derivatives (**1c–5c**), were synthesized and evaluated by NMR spectroscopic studies for their structure determination. These dyes were implemented on polyester fabric by Thermosol dyeing and evaluated by colorfastness tests. They were further tested by conducting experimental solvatochromism as well as computational studies. These dyes were also checked for their antibacterial activity, and computational studies performed by TD-SCF DFT and molecular docking.

2. Experimental

2.1. Material and methods

All chemicals utilized in this study (aldehydes, aluminum chloride hexahydrate, alumina, hydrazine, and amines) and solvents (including chloroform, acetonitrile, methanol, ethyl acetate, acetic acid, and *n*-hexane) were purchased from Sigma-Aldrich with 99% purity. The reaction progress and purity were checked using thin layer chromatography plates (Merck company) pre-coated with silica on aluminium sheets.

2.2. Synthesis procedure

The azodiene (**1a–5a**) and azodienophile (**1b–5b**) precursors were synthesized by using aromatic aldehydes (4 mM, 0.7 mg), hydrazine monohydrate (2 mM, 100 μL) and aromatic-substituted hydrazine (2 mM, 0.396 mg) in a 2 : 1 and 1 : 1 ratio, respectively. This synthesis was carried out in acetonitrile solvent at room temperature with constant magnetic stirring. To obtain a good yield, acetic acid was used as a catalyst. Then, by using solvent-free and green grindstone synthesis, some novel 1,2,4-triazine derivatives (**1c–5c**) were prepared (Scheme 1 and Table 1). For this, azodiene (0.1 mM, 0.328 mg) (**1a–5a**) and azodienophile (0.1 mM, 0.164 mg) (**1b–5b**) in a 1 : 1 ratio were mixed and ground with a mortar and pestle for about 20–30 min at room temperature (30 °C). In these reactions, a Lewis acid ($AlCl_3{\cdot}6H_2O$) 0.1 mM (0.241 mg) was used as a catalyst and alumina 0.3 mM (0.306 mg) as a solid support. The reaction progress was checked by physical appearance, melting point and TLC plates. After satisfactory observation, this reaction mixture was dissolved in acetonitrile (or chloroform) to obtain the 1,2,4-triazine derivatives (**1c–5c**). The required products were found in the filtrate. Finally, the solvent was evaporated and 1,2,4-triazines were collected in crystalline or powder form.

2.3. Characterization

2.3.1. 3,6-Bis(4-chlorophenyl)-5-(3,4-dimethoxyphenyl)-*N*-(2,4-dinitrophenyl)-5,6-dihydro-1,2,4-triazin-4(3*H*)-amine (1c). Physical appearance: dark-red powder; M.P: 163 °C; ^{1}H NMR ($CDCl_3$, 400 MHz): δ (ppm) 8.83 (1H, s, H-3), 5.50 (1H, d, H-5), 4.25 (1H, d, H-6), 8.85 (1H, s, H-7), 7.90 (1H, s, H-10), 7.88 (1H, d, H-12), 7.45 (1H, d, H-13), 7.99 (1H, d, H-2′), 7.66 (1H, d, H-3′), 7.66 (1H, d, H-5′), 7.99 (1H, d, H-6′), 7.66 (1H, d, H-2″), 7.99 (1H, d, H-3″), 7.35 (1H, d, H-5″), 7.28 (1H, d, H-6″), 6.90 (1H, s, H-2‴), 3.86 (3H, s, 3a‴–OCH_3), 3.86 (3H, s, 4a‴–OCH_3), 6.90 (1H, d, H-5‴), 6.91 (1H, d, H-6‴); ^{13}C NMR ($CDCl_3$, 100 MHz): δ 60.6 (C-3), 60.5 (C-5), 60.4 (C-6), 161.2 (C-8), 130.9 (C-9), 123.6 (C-10), 144.7 (C-11), 130.9 (C-12), 108.3 (C-13), 144.7 (C-1′), 129.4 (C-2′), 129.2 (C-3′), 130.9 (C-4′), 129.2 (C-5′), 129.4 (C-6′), 144.7 (C-1″), 129.8 (C-2″), 126 (C-3″), 130.9 (C-4″), 126 (C-5″), 129.8 (C-6″), 130.9 (C-1‴), 110.9 (C-2‴), 149.6 (C-3‴), 56 (C-3a‴), 148 (C-4‴), 56 (C-4a‴), 122.8 (C-5‴), 116.6 (C-6‴); EI-MS: *m*/*z* 622.1(for $C_{29}H_{24}Cl_2N_6O_6$).

2.3.2. 4,4′-(5-(3,4-Dimethoxyphenyl)-4-((2,4-dinitrophenyl)-amino)-3,4,5,6-tetrahydro-1,2,4-triazine-3,6-diyl)diphenol (2c). Physical appearance: dark-red powder; M.P: 236 °C–237 °C; ^{1}H NMR ($CDCl_3$, 500 MHz): δ 8.84 (1H, s, H-3), 4.28 (1H, d, H-5), 4.26 (1H, d, H-6), 8.69 (1H, s, H-7), 8.84 (1H, s, H-10), 7.90 (1H, d, H-12), 7.38 (1H, d, H-13), 7.90 (1H, d, H-2′), 7.88 (1H, d, H-3′), 8.89 (1H, s, 4a′-OH), 7.88 (1H, d, H-5′), 7.90 (1H, d, H-6′), 7.29 (1H, d, H-2″), 6.75 (1H, d, H-3″), 8.89 (1H, s, 4a″-OH), 6.75 (1H, d, H-5″), 7.29 (1H, d, H-6″), 6.90 (1H, s, H-2‴), 3.86 (3H, s, 3a‴–OCH_3), 3.86 (3H, s, 4a‴–OCH_3), 6.90 (1H, d, H-5‴), 6.91 (1H, d, H-6‴); ^{13}C NMR ($CDCl_3$, 125 MHz): δ 60.9 (C-3), 60.5 (C-5), 60.2 (C-6), 161.2 (C-8), 130 (C-9), 123.6 (C-10), 144.7 (C-11), 130 (C-12), 108.4 (C-13), 130 (C-1′), 130 (C-2′), 116.6 (C-3′), 165 (C-4′), 116.6 (C-5′), 130 (C-6′), 130 (C-1″), 130 (C-2″), 116.6 (C-3″), 164 (C-4″), 116.6 (C-5″), 130 (C-6″), 130 (C-1‴), 110.9 (C-2‴), 149.1 (C-3‴), 56 (C-3a‴), 148.1 (C-4‴), 56 (C-4a‴), 122.8 (C-5‴), 116.6 (C-6‴); EIMS: *m*/*z* 586.18 ($C_{29}H_{26}N_6O_8$).

2.3.3. 4,4′-(5-(3,4-Dimethoxyphenyl)-4-((2,4-dinitrophenyl)-amino)-3,4,5,6-tetrahydro-1,2,4-triazine-3,6-diyl)bis(2-methoxyphenol) (3c). Physical appearance: dark-red powder; M.P: 159 °C–162 °C; ^{1}H NMR ($CDCl_3$, 500 MHz): δ 8.84 (1H, s, H-3), 5.69 (1H, d, H-5), 4.57 (1H, d, H-6), 8.84 (1H, s, H-7), 8.85 (1H, s, H-10), 7.90 (1H, d, H-12), 7.88 (1H, d, H-13), 7.90 (1H, s, H-2′), 3.85 (3H, s, 3a′–OCH_3), 8.85 (1H, s, 4a′-OH), 6.86 (1H, d, H-5′), 6.78 (1H, d, H-6′), 6.85 (1H, s, H-2″), 3.85 (3H, s, 3a″–OCH_3), 8.85 (1H, s, 4a″-OH), 6.89 (1H, d, H-5″), 6.78 (1H, d, H-6″), 7.16 (1H, s, H-2‴), 3.86 (3H, s, 3a‴–OCH_3), 3.86 (3H, s, 4a‴–OCH_3), 6.91 (1H, d, H-5‴), 6.98 (1H, d, H-6‴); ^{13}C NMR: ($CDCl_3$, 125 MHz): δ 60.9 (C-3), 60.5 (C-5), 60.2 (C-6), 161.2 (C-8), 130 (C-9), 123.6 (C-10), 144.7 (C-11), 130 (C-12), 108.4 (C-13), 130.1 (C-1′), 116.6 (C-2′), 148.1 (C-3′), 56 (C-3a′), 144.7 (C-4′), 116.6 (C-5′), 122.8 (C-6′), 130.1 (C-1″), 116.6 (C-2″), 148.1 (C-3″), 144.7 (C-4″), 116.6 (C-5″), 122.8 (C-6″), 129.9 (C-1‴), 110.9 (C-2‴), 149.1 (C-3‴), 56 (C-3a‴), 148.1 (C-4‴), 56 (C-4a‴), 122.8 (C-5‴), 116.6 (C-6‴); EIMS: *m*/*z* 646.21 ($C_{31}H_{30}N_6O_{10}$).

2.3.4. 3,5,6-Tris(3,4-dimethoxyphenyl)-*N*-(2,4-dinitrophenyl)-5,6-dihydro-1,2,4-triazin-4(3*H*)-amine (4c). Physical appearance: reddish crystalline form; M.P: 254 °C–256 °C; ^{1}H NMR ($CDCl_3$, 400 MHz): δ 8.84 (1H, s, H-3), 5.53 (1H, d, H-5), 4.29 (1H, d, H-6), 8.84 (1H, s, H-7), 8.85 (1H, s, H-10), 7.38 (1H, d, H-12), 7.36 (1H, d, H-13), 6.88 (1H, s, H-2′), 3.86 (3H, s, 3a′–OCH_3), 3.86 (3H, s, 4a′–OCH_3), 6.91 (1H, d, H-5′), 6.90 (1H, d, H-6′), 6.88 (1H, s, H-2″),

 © 2025 The Author(s). Published by the Royal Society of Chemistry

Open Access Article. Published on 19 August 2025. Downloaded on 3/29/2026 11:26:00 PM.
This article is licensed under a Creative Commons Attribution-NonCommercial 3.0 Unported Licence.

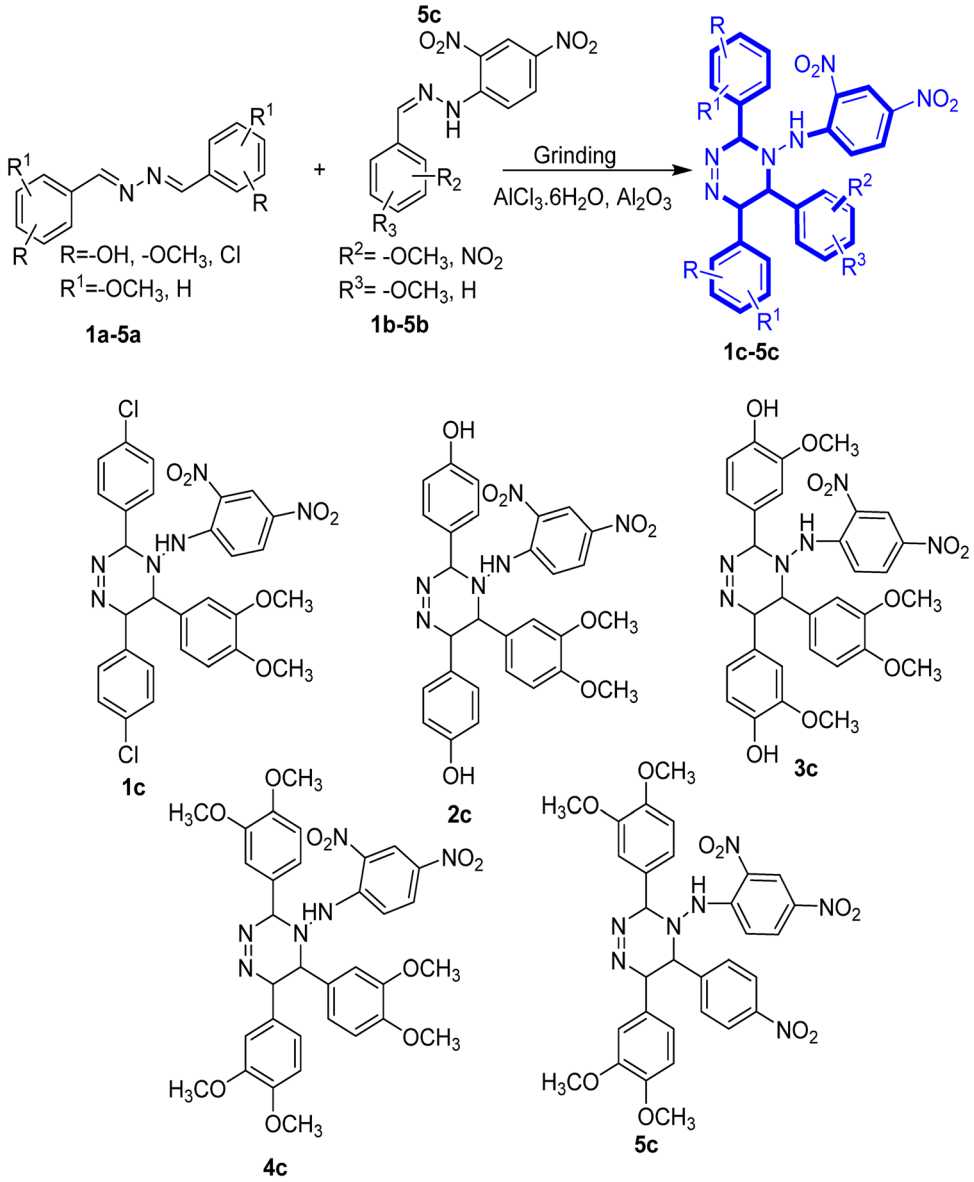

Scheme 1 Synthesis of novel 1,2,4-triazine dyes (**1c–5c**).

3.86 (3H, s, 3a″–OCH_3), 3.86 (3H, s, 4a″–OCH_3), 6.91 (1H, d, H-5″), 6.90 (1H, d, H-6″), 6.89 (1H, s, H-2‴), 3.86 (3H, s, 3a‴–OCH_3), 3.86 (3H, s, 4a‴–OCH_3), 7.13 (1H, d, H-5‴), 7.36 (1H, d, H-6‴); ^{13}C NMR: ($CDCl_3$, 100 MHz): δ 60.9 (C-3), 60.5 (C-5), 60.2 (C-6), 151.9 (C-8), 137.9 (C-9), 123.6 (C-10), 137.9 (C-11), 129.9 (C-12), 108.3 (C-13), 137.9 (C-1′), 116.6 (C-2′), 149.6 (C-3′), 56 (C-3a′), 148.1 (C-4′), 56 (C-4a′), 116.6 (C-5′), 122.8 (C-6′), 137.9 (C-1″), 116.6 (C-2″), 149.6 (C-3″), 56 (C-3a″), 148.1 (C-4″), 56 (C-4a″), 116.6 (C-5″), 122.8 (C-6″), 129.9 (C-1‴), 110.9 (C-2‴), 149.1 (C-3‴), 56 (C-3a‴), 148.1 (C-4‴), 56 (C-4a‴), 122.8 (C-5‴), 123.6 (C-6‴); EI-MS: *m*/*z* 675.2 (for $C_{33}H_{34}N_6O_{10}$).

2.3.5. 3,6-Bis(3,4-dimethoxyphenyl)-*N*-(2,4-dinitrophenyl)-5-(4-nitrophenyl)-5,6-dihydro-1,2,4-triazin-4(3*H*)-amine (5c). Physical appearance: yellowish needle-like crystals; M.P: 285 °C–288 °C; ^{1}H NMR ($CDCl_3$, 500 MHz): δ 8.84 (1H, s, H-3), 5.53 (1H, d, H-5), 5.50 (1H, d, H-6), 8.84 (1H, s, H-7), 8.85 (1H, s, H-10), 7.90 (1H, d, H-12), 7.56 (1H, d, H-13), 6.96 (1H, s, H-2′), 3.86 (3H, s, 3a′–OCH_3), 3.86 (3H, s, 4a′–OCH_3), 6.88 (1H, d, H-5′), 6.95 (1H, d, H-6′), 6.96 (1H, s, H-2″), 3.86 (3H, s, 3a″–OCH_3), 3.86 (3H, s, 4a″–OCH_3), 6.88 (1H, d, H-5″), 6.95 (1H, d, H-6″), 7.55 (1H, d, H-2‴), 8.29 (1H, d, H-3‴), 8.29 (1H, d, H-5‴), 7.55 (1H, d, H-6‴); ^{13}C NMR: ($CDCl_3$, 125 MHz): δ 70.5 (C-3), 70.5 (C-5), 60.5 (C-6), 152 (C-8), 138 (C-9), 110.6 (C-10), 138 (C-11), 110.3 (C-12), 108.8 (C-13), 137.9 (C-1′), 110.6 (C-2′), 149.4 (C-3′), 56 (C-3a′), 149 (C-4′), 56 (C-4a′), 121 (C-5′), 110.6 (C-6′), 134 (C-1″), 110.6 (C-2″), 149.4 (C-3″), 56 (C-3a″), 149 (C-4″), 56 (C-4a″), 121 (C-5″), 110.6 (C-6″), 144 (C-1‴), 126.8 (C-2‴), 124.2 (C-3‴), 149.4 (C-4‴), 124.2 (C-5‴), 126.8 (C-6‴); EI-MS: *m*/*z* 659.20 (for $C_{31}H_{29}N_7O_{10}$).

2.4. Material application as dyeing

2.4.1. Application procedure. The disperse method was used for dyeing 100% polyester. Dye solution (0.01 g/100 mL)

Open Access Article. Published on 19 August 2025. Downloaded on 3/29/2026 11:26:00 PM.
This article is licensed under a Creative Commons Attribution-NonCommercial 3.0 Unported Licence.

Table 1 Colorfastness evaluation of dye compounds (**1c–5c**). Colorfastness to washing ISO 105-C06-A2S and ISO 105-E01

Dye compound	Color	Fabric types					
		Acetate	Cotton	Nylon	Polyester	Acrylic	Wool
1c		4-5	4-5	4-5	4-5	4-5	4-5
2c		4-5	4-5	4-5	4-5	4-5	4-5
3c		4-5	4-5	4-5	4-5	4-5	4-5
4c		4-5	4-5	4-5	4-5	4-5	4-5
5c		4-5	4-5	4-5	4-5	4-5	4-5

Colorfastness to perspiration (acidic & alkaline) ISO 105-E04

Dye compound	Fabric types					
	Acetate	Cotton	Nylon	Polyester	Acrylic	Wool
1c	4-5	4-5	4-5	4-5	4-5	4-5
2c	4-5	4-5	4-5	4-5	4-5	4-5
3c	4-5	4-5	4-5	4-5	4-5	4-5
4c	4-5	4-5	4-5	4-5	4-5	4-5
5c	4-5	4-5	4-5	4-5	4-5	4-5

Dye compound	Colorfastness to rubbing ISO 105-X12	
	DRY	WET
1c	4-5	4-5
2c	4-5	4-5
3c	4-5	4
4c	4-5	4-5
5c	4	4

Dye compound	Colorfastness to light (xenon arc lamp) 12 hours (blue scale reading)
S1 or **1c**	1-2
S2 or **2c**	1-2
S3 or **3c**	1
S4 or **4c**	1
S21 or **5c**	4

was pad on 100% polyester fabric, which had a pick-up of almost 70% at room temperature. The dyed fabric was dried at 100 °C and cured at 200 °C in a curing machine for about 1 min. Caustic soda (4 g L^{-1}) and sodium hydrosulphite (4 g L^{-1}) at a liquor ratio of 1 : 10 were used to clear the reduction from the fabric.

2.4.2. Colorfastness assessment. Colorfastness tests (perspiration, rubbing, light, and washing) were performed according to ISO standard procedures. The ISO 105-C06 testing protocol was used for washing. The reference detergent WOB was used to prepare washing liquor in 4 g L^{-1} water using AATCC. In a stainless steel container, this detergent along with the composite specimen (dyed fabric tied with control fabric) was used for laundry purpose at a temperature of less than 60 °C. Then, it was washed out for 1–2 min in 100 mL water two times and dried, and then compared with the grey scale. The ISO 105-X 12 protocols were applied for rubbing. A crock meter concluded the dry rubbing with a downward force at a rate of 1 cycle s^{-1} for twenty times under atmospheric conditions, *i.e.* 20 °C ± 2 °C temp. and 65% ± 2% relative humidity. In the case of wet rubbing, a similar process was applied. The ISO 105-B02 method explained the effect of UV-light under a xenon arc lamp for 12 h on the dyed fabric. Colorfastness to perspiration (acidic and basic) was observed using the ISO 105-E04 process. In this process, a piece of dyed fabric was soaked in synthetic perspiration solution for 30 min. To check the staining and changing dye color, the soaked dyed fabric and control fabric were placed under the testing device at standard pressure. Finally, the grey scale was used for comparison of all the tested samples.

 © 2025 The Author(s). Published by the Royal Society of Chemistry

Open Access Article. Published on 19 August 2025. Downloaded on 3/29/2026 11:26:00 PM.
This article is licensed under a Creative Commons Attribution-NonCommercial 3.0 Unported Licence.

2.5. Solvent effect (solvatochromism) and UV-visible light effect (photochromism) study on the dye solutions

To observe solvatochromism, different solvents with varying polarity were used to dissolve the targeted molecules (**1c–5c**) such as DMSO, acetonitrile, DCM, chloroform, and ethyl acetate. For the evaluation of the UV-visible λ_{max} value of each solution, a double-beam spectrophotometer was used. To explore the data, graphs were plotted with the help of the Origin software. In addition, the experimental data was compared with the theoretical data. The effect of photochromism on all dye solutions was seen under sunlight and picked up in the images. Then, these solutions were placed under UV-fluorescence light to observe any change in color.

2.6. Antibacterial investigation

The disc diffusion method was used to evaluate the bactericidal potential of the target compounds, namely **1c–5c**. Agar medium was transferred to an autoclave machine to kill infectious agents and avoid contamination. Then, sterilized Petri dishes were placed in a disinfected environment and labeled. The agar solution was poured into Petri dishes and left to solidify. Then, 100 μL bacterial broth solution was spread on the agar dishes with the help of an autoclaved spreader. These Petri dishes were covered for 20 min and left under laminar flow at 37 °C. The dyed fabric pieces were placed on nutrient agar plates carefully. Alternatively, cephalosporin was used as a positive control. Then, the Petri plates were sealed with plastic cling and placed in an incubator for 24 h at 37 °C. After 24 h, the samples were checked for the presence of any inhibition zones, and their size was measured in millimeters (mM).[27]

2.7. Computational study of structure–activity relationship

2.7.1. Molecular docking analysis. Molecular docking of the targeted compounds (**1c–5c**) was observed using the Molegro Virtual Docker (MVD) software to explore the experimental results against bacterial action. For this action, binder proteins, *i.e.* 4WK1 and 1JIL of *Escherichia coli* and *Staphylococcus aureus* (because the same strains were experimentally tested), respectively, were downloaded from the Protein Data Bank (**https://www.rcsb.org/**) in PDB:ID format. Cephalosporin was used as the reference drug for bacterial action and downloaded in the form of 2D structure SDF format from PubChem. Cephalosporin and all the targeted compounds before docking were stabilized using Chem3D (PerkinElmer) to minimize energy by MM4 and MMFF94. Then, cephalosporin and all ligands were saved in mol2 format for the Molegro software. In the Molegro workspace, firstly protein was imported and prepared with the removal of cofactors, water molecules with no warnings. Then, cavities were detected in the protein and a surface was created. After that, the active ligand of the protein was changed into a cofactor and all remaining protein ligands were removed from the workspace. Subsequently, ligands (**1c–5c**) were imported into the workspace and prepared one by one. Later, Docking Wizard for protein–ligand interaction was selected in all poses. The best pose suggested the hydrogen bond interaction and greatest MolDock score. The BIOVIA Discovery studio visualizer was used to visualize the best pose of all the interactions in the form of 3D and 2D images.[28]

2.7.2. Quantum chemical studies and photophysical parameter determination using DFT/TD-DFT. Density functional theory (DFT) was performed to explain the quantum studies such as electronegativity, HOMO and LUMO energy gap, electron affinity, chemical hardness, nucleophilicity index, chemical softness and electrophilicity index of the compounds (**1c–5c**). Two theories, *i.e.* frontier molecular orbitals and molecular electrostatic potential, explained the structure activity relationship of these compounds. Gaussian 09 (version D.01) was used to perform all the DFT calculations (quantum studies).[29] For the optimization of these compounds, B3LYP ground state-DFT (method) and 6311G (basis set) were used to determine the quantum chemical data. To determine the absorption characteristics of different solvents (DMSO, acetonitrile, DCM, chloroform, and ethyl acetate), the IEFPCM model (integral equation formalism polarizable continuum model) was applied. Then the absorption graphs of the various solvents were plotted on Origin 2019b (version 9.65) (**https://www.originlab.com**).[30]

2.7.3. Hirshfeld analysis of surface region participation in fabric interactions. The crystallographic computational approach with the 6-311G basis set and B3LYP method employed to assess the intermolecular interactions within the structure of a crystal is known as Hirshfeld surface analysis. It emphasizes interaction zones through the formation of a surface with three dimensions around a molecule based on its electron density contribution. To interpret the types of interactions, surface regions are mapped with attributes such as shape ratio and electrostatic potential. These surfaces offer 2D fingerprint plots, which are helpful in displaying and characterizing interactions such as van der Waals forces, π–π stacking, and hydrogen bonding. Materials science, biopharmaceutical solid-state assessment, and crystal engineering all significantly employ this technique. The Multiwfn 3.7 software and Crystal Explorer were used to analyze the Hirshfeld surface, where the program imported the Gaussian-formatted checkpoint of the geometry-optimized structure. Real-space functions were calculated such as shape index and curvedness of the analysis to explain the intermolecular interactions in visual form. The molecular surface was generated and the interaction parameters were charted and plotted using the in-built visualisation tools. Then, the surfaces were transferred to VMD where they can be graphically shown as interaction hotspots and other packing properties. This was carried out through the structural analysis of the crystal form, in which its intermolecular hydrogen bonding and p–i stacking were noted.

3. Results and discussion

3.1. Organic synthesis and characterization

The synthetic approach used in this study is shown in Scheme 1 and the novelty of the method lies in the use of the grindstone method in combination with a Friedel–Crafts reaction, in

Open Access Article. Published on 19 August 2025. Downloaded on 3/29/2026 11:26:00 PM.
This article is licensed under a Creative Commons Attribution-NonCommercial 3.0 Unported Licence.

which a Lewis acid is used as a catalyst. However, in the one-pot multi-component strategy, a two-method strategy was employed in a synergistic combination. The structures of the synthesized compounds were identified by spectroscopic analysis using ^{1}H-, ^{13}C-NMR and EIMS (Fig. S1–S6: SI). The ^{1}H-NMR spectral data of **1c** displayed one singlet at δ 8.83 ppm and two doublets at δ 5.50 and 4.25 ppm, corresponding to protons belonging to the main triazine core. A singlet at δ 8.85 ppm was observed in the ^{1}H-NMR spectrum of **1c**, which confirmed the presence of an –N–NH– linkage in the molecule, confirming the-azo-coupling. Further, a singlet at δ 7.90 ppm and two doublets at δ 7.88 and 7.45 ppm were observed in its ^{1}H-NMR spectrum, corresponding to a 2,4-dinitrobenzene ring. Additionally, four doublets of double intensity were also found in the spectrum, corresponding to a bi-phenyl

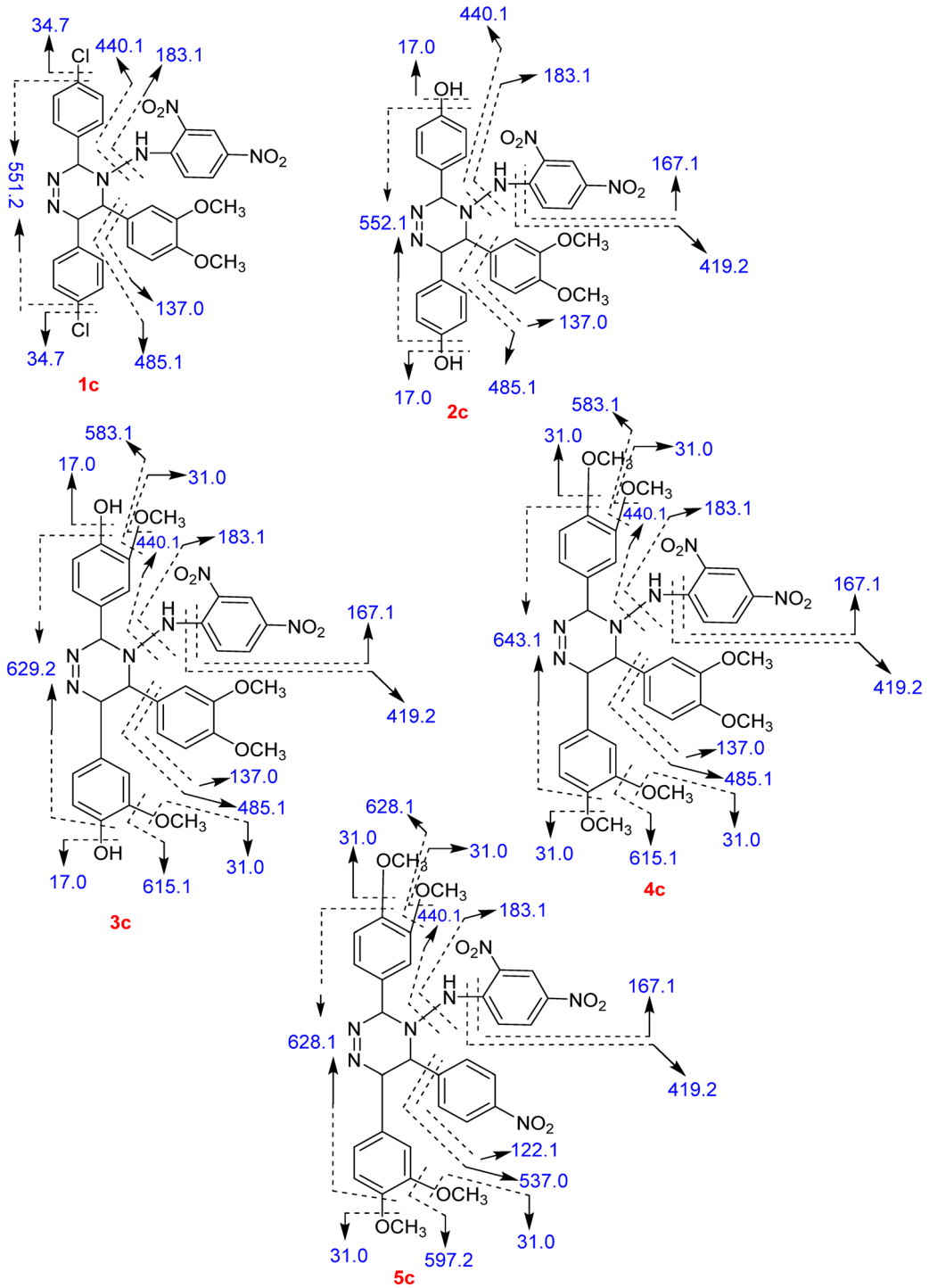

Fig. 1 EI-MS fragmentation of compounds **1c–5c**.

 © 2025 The Author(s). Published by the Royal Society of Chemistry

Open Access Article. Published on 19 August 2025. Downloaded on 3/29/2026 11:26:00 PM.
This article is licensed under a Creative Commons Attribution-NonCommercial 3.0 Unported Licence.

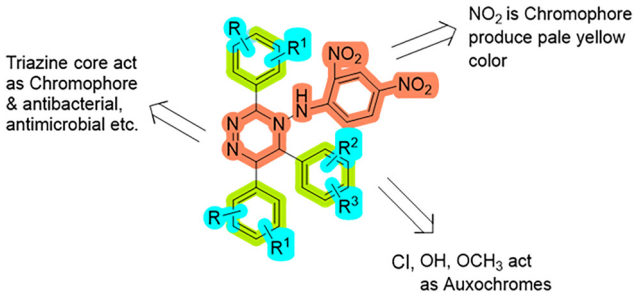

Fig. 2 Structure–activity relationship of target compounds (**1c–5c**).

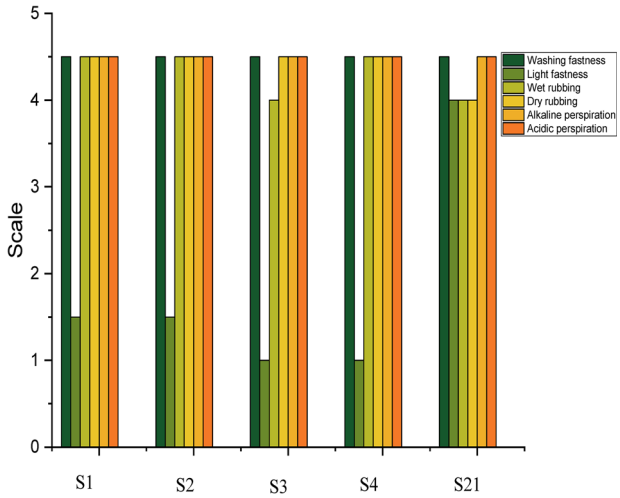

Fig. 3 Colorfastness assessment of target compounds (**1c–5c**) [**1c** = **S1**, **2c** = **S2**, **3c** = **S3**, **4c** = **S4** and **5c** = **S21**].

system. Two singlets were observed at δ 3.86 ppm, which correspond to the $-OCH_3$ groups, and also confirmed by the downfield signals at δ 149.6 (C-3‴) and 148 (C-4‴) ppm in the ^{13}C-NMR spectrum, corresponding to the quaternary carbon to with these methoxy groups are attached. Further, the carbon signals at δ 56.0 ppm also confirmed the presence of methoxy groups in the **1c** molecule. The ^{13}C-NMR spectral data was also found to be in accordance with and supported by the ^{1}H-NMR spectral analysis. The EI-MS data of **1c** displayed evidence for confirmation of the product with molecular formula (M^+ 183). The fragment peak at m/z 369.2 refers to the $-N-NH-C_6H_3(NO_2)_2$ fragment (Fig. 1). The spectral data of **2c** was found to be similar to that of **1c** except for the presence of two signals at δ 8.89 ppm (1H, s, 4a″-OH) and δ 8.89 ppm (1H, s, 4a′-OH) for the hydroxyl group in its ^{1}H-NMR spectrum and supported by the signals at δ 164 (C-4″) and 165 ppm (C-4′) in its ^{13}C-NMR spectrum, which confirmed the presence of hydroxyl and absence of –chloro groups. This was additionally evidenced by the EI-MS data, which also confirmed the presence of hydroxyl groups at m/z 552.1 due to the fragmented hydroxyl. Similarly, the spectral analysis of **3c**, **4c** and **5c** was also found to be the same except for the differences observed for the presence of $-OCH_3$ in **3c**, absence of hydroxyl and presence of $-OCH_3$ in **4c**, whereas **5c** was found to be very close to **4c** in spectral analysis with the absence of an $-NO_2$ group (Fig. 1).

3.2. Chemistry

Azo dye compounds such as 1,2,4-triazine and its derivatives play an important role in the textile industry. They also have many applications in biological systems and medicinal chemistry. They form covalent bonds under alkaline conditions between the carbon atom of the dye compound and hydroxyl group of cellulose fibers. To achieve colorfastness, monochlorotriazine and dichlorotriazine are commonly used as reactive

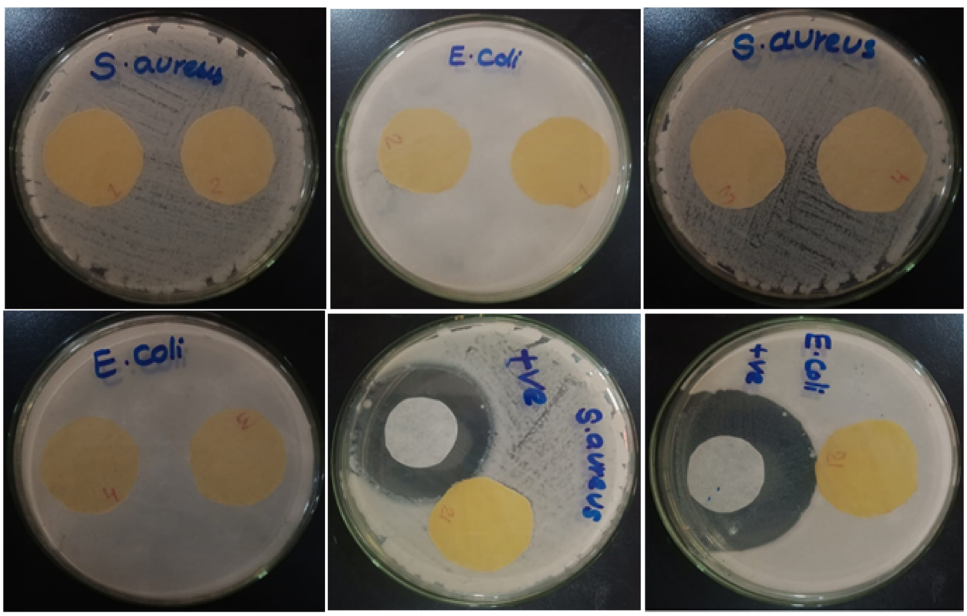

Fig. 4 Measurement of inhibition zone. Experimental representation of the antibacterial activity of bacterial strains for the synthesized compounds loaded on fabric as dyes.

Open Access Article. Published on 19 August 2025. Downloaded on 3/29/2026 11:26:00 PM.
This article is licensed under a Creative Commons Attribution-NonCommercial 3.0 Unported Licence.

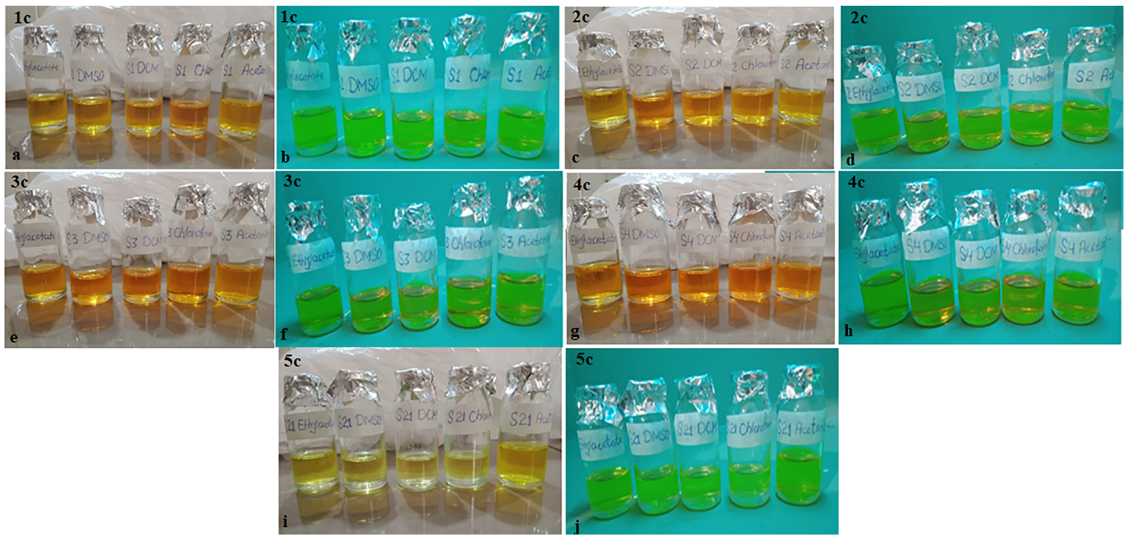

Fig. 5 Influence of UV-visible light and sunlight on the color change (in different solvents) of the target molecules (**1c–5c**).

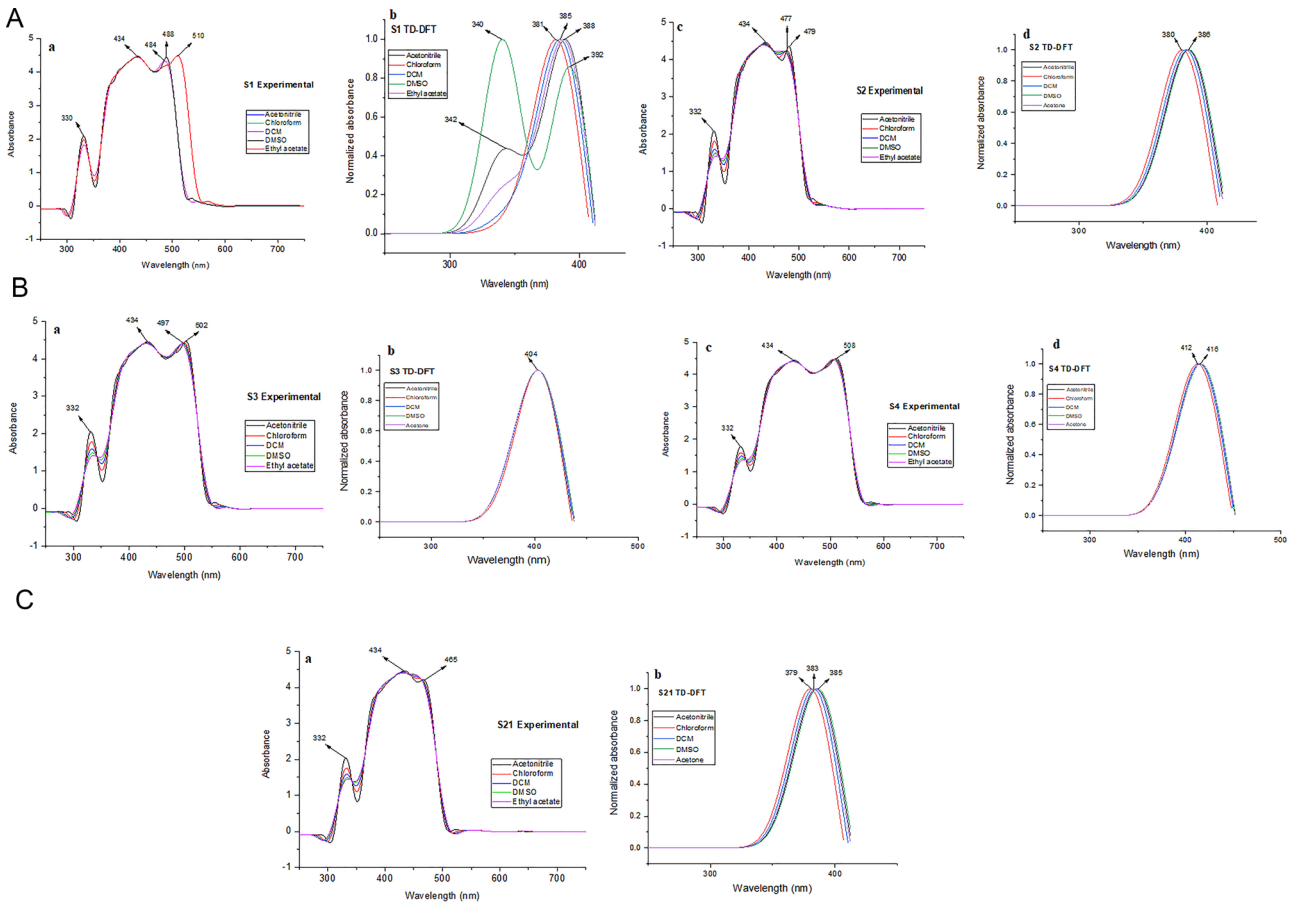

Fig. 6 (A) Experimental and theoretical analysis of optical properties by solvatochromism and photochromism of target compounds **1c–2c** (where **S1** = **1c** and **S2** = **2c**). (B) Experimental and theoretical analysis of optical properties by solvatochromism and photochromism of target compounds **3c–4c** (where **S3** = **3c** and **S4** = **4c**). (C) Experimental and theoretical analysis of optical properties by solvatochromism and photochromism of target compound **5c** (where **S21** = **5c**).

dyes.[31] In the case of polyester, the $-NO_2$ group is an electron-withdrawing group used in disperse dyes and capable of inducing pale-yellow color. Electron-donating groups such as chloro, hydroxy and methoxy ($-OCH_3$) groups enhance the

 © 2025 The Author(s). Published by the Royal Society of Chemistry

Open Access Article. Published on 19 August 2025. Downloaded on 3/29/2026 11:26:00 PM.
This article is licensed under a Creative Commons Attribution-NonCommercial 3.0 Unported Licence.

bactericidal factor and act as auxochromes (Fig. 2). Triazine derivatives functionalized with NO_2, Cl, OH, or OCH_3 groups exhibit distinct biological activities due to their electronic and steric properties. Nitro (NO_2)-substituted triazines demonstrate notable antibacterial and antifungal effects,[32] given that the electron-withdrawing nature of NO_2 disrupts microbial electron transport chains. Chloro (Cl) groups enhance the broad-spectrum antimicrobial activity[30,33] against drug-resistant strains by alkylating pathogen DNA. Hydroxyl (OH)-bearing triazines show anticancer potential,[34] particularly in breast and colon cancer cell lines, by inducing oxidative stress and apoptosis. Methoxy ($-OCH_3$) substitutions improve antifungal bioavailability by increasing the lipophilicity, aiding penetration into fungal cell membranes. The triazine core itself acts as a pharmacophore, enabling synergistic interactions with biological targets.[35]

In this study, all the compounds (**1c**–**5c**) have the same central part (core), which resisted bacterial growth, and also acted as a chromophore due to conjugation of electrons. In **1c**, the chloro and methoxy groups attached to its phenyl ring resist bacterial growth and act as an auxochrome, and thus no bacterial growth was observed on polyester fabric. The nitro groups on substituted hydrazine reveal yellow color. In **2c**, **3c**,

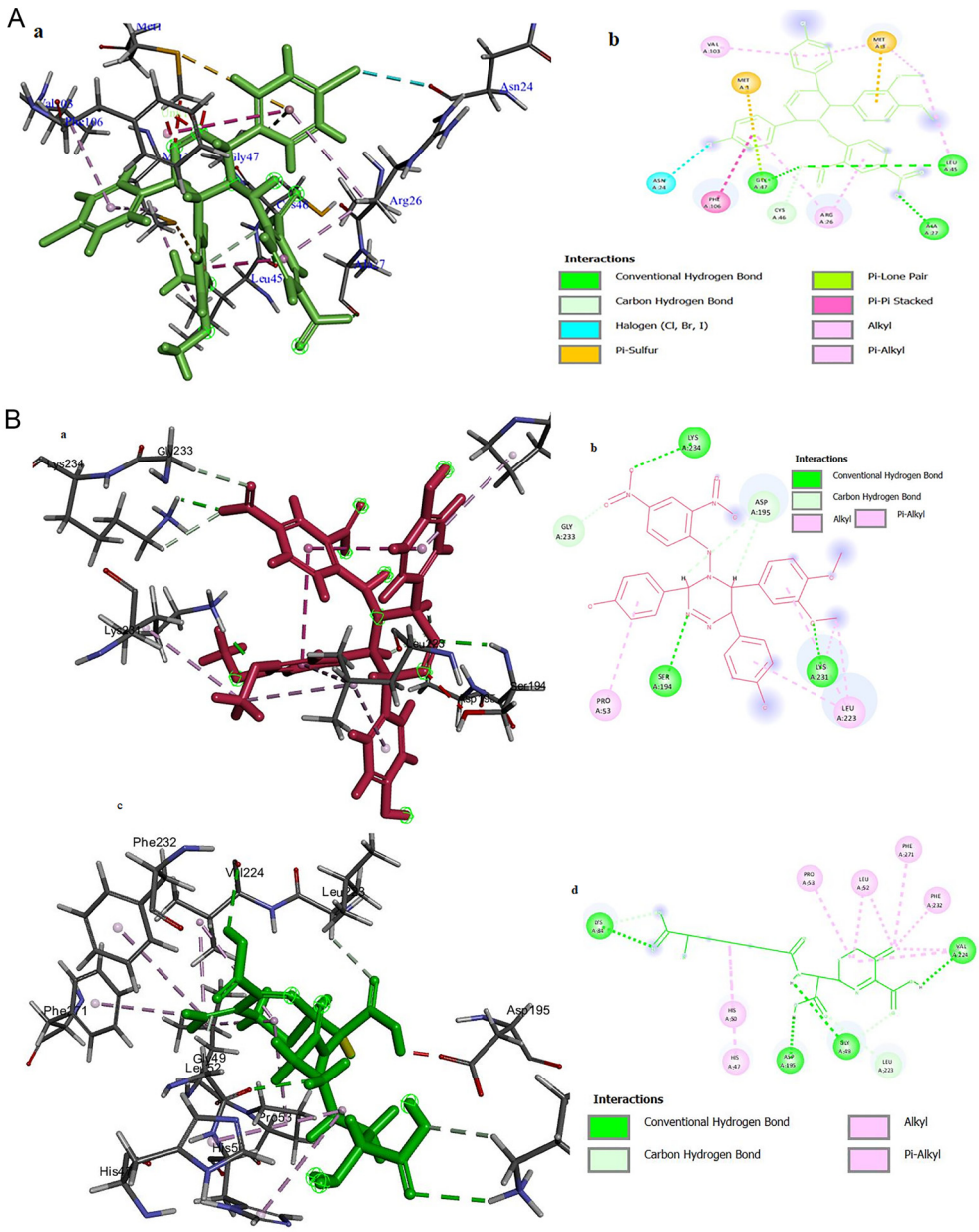

Fig. 7 (a) 3D interaction of **1c** in complex with 4WK1; (b) 2D-interaction of **1c** in complex with 4WK1; (c) 3D interaction of cephalosporin (reference drug) in complex with 4WK1; and (d) 2D interaction of cephalosporin (reference drug) in complex with 4WK1. (b) (a) 3D interaction of **2c** in complex with 1JIL; (b) 2D-interaction of **2c** in complex with 1JIL; (c) 3D interaction of cephalosporin (reference drug) in complex with 1JIL; and (d) 2D interaction of cephalosporin (reference drug) in complex with 1JIL.

Open Access Article. Published on 19 August 2025. Downloaded on 3/29/2026 11:26:00 PM.
This article is licensed under a Creative Commons Attribution-NonCommercial 3.0 Unported Licence.

and **4c**, the methoxy and hydroxy groups attached to the phenyl ring resist bacterial growth, as mentioned in the literature.[36] Alternatively, in **5c**, it possesses one more nitro group compared to the others, which revealed bright-yellow color on polyester fabric.

3.3. Application of dyes on fabric

3.3.1 Colorfastness analysis. Colorfastness to washing and perspiration (acidic and basic) on multiple fabrics (such as acetate, cotton, nylon, polyester, acrylic, and wool), rubbing (wet and dry), and light was examined by standard methods (Fig. 3). These methods were applied to the dye compounds (**1c–5c**). The dye compounds (**1c–5c**) were observed to have very good results according to the grey scale rating of 4–5 in colorfastness to washing, perspiration, and rubbing. In contrast, the dye compounds (**1c–5c**) showed poor lightfastness results with a rating of 1–2 under a Xenon arc lamp for 12 h. Nevertheless, dye **5c** showed moderate results with a rating of 4 according to the blue scale (Table 1).

The colorfastness of the triazine-based dyes, as depicted in Fig. 3, is highly dependent on the nature of their substituents. The NO_2 group improves the light-fastness due to its UV-absorbing capability but may reduce the wash-fastness owing to its polar nature.[37] Chlorine substituents enhance both the wash and rub fastness by forming strong covalent bonds with textile fibers. Methoxy ($-OCH_3$) groups contribute to moderate light fastness and excellent wet fastness due to their hydrophobic character. The triazine core further enhances fixation on fabrics through reactive bonding with cellulose, making these dyes highly durable under industrial conditions.[38,39]

3.3.4. Antibacterial activity. The antibacterial activity of novel triazine derivatives such as 3-[(pyridine-2-ylamino)-methyl]1,6-dihydro-1,2,4-triazine-5(2*H*)-one and 3-[(pyridine-2-ylamino)methyl]1,6-dihydro-1,2,4-triazine-5(2*H*)-one were checked against Gram-positive bacteria (*Bacillus cereus*, *Staphylococcus aureus*, and *Enterococcus faecalis*) and Gram-negative bacteria (*Pseudomonas aeruginosa*, *Escherichia coli* and *Klebsiella pneumoniae*) compared to the reference drugs amoxicillin and ceftriaxone. These derivatives have potential as antibacterial drugs.[40]

In the current study, the antibacterial activity was assessed using the disc diffusion method against *Escherichia coli* and *Staphylococcus aureus*. The results clearly predicted that the dyed fabrics using the synthesized dyes (**1c–5c**) have significant resistance against bacterial growth. No bacteria growth was observed on the upper and lower part of the dyed fabrics after 24 h at 37 °C. Around the dyed fabric samples, no inhibition zone was created, which indicated that no leaching of the dyes occurred on the fabrics (Fig. 4). This is the advantage of our target compounds (**1c–5c**), which develop strong interactions with the textile fibers, leading to the good fixation and levelness of the dye on the fibers. These results suggested that the synthesized dyes have potential against bacterial growth. It has been reported that the triazine core possesses a dual nature as an antibacterial and color-imparting chromophore. Therefore, our target compounds (**1c–5c**) not only have anti-bacterial potential but also have excellent fixation with textile fibers. This collection of characteristics not only saves money but also time (for a number of applications), leading to a cost-effective strategy. Moreover, the substituents such as chloro, nitro, and hydroxy present on the dye-compounds (**1c–5c**) also participate in enhancing their bacterial activity. Chloro-substituted triazine creates a strong electrostatic interaction with the bacterial DNA. This causes the leakage of potassium from bacterial cells, depolarizing the cell membrane and leading to bacterial cell death.[40,41]

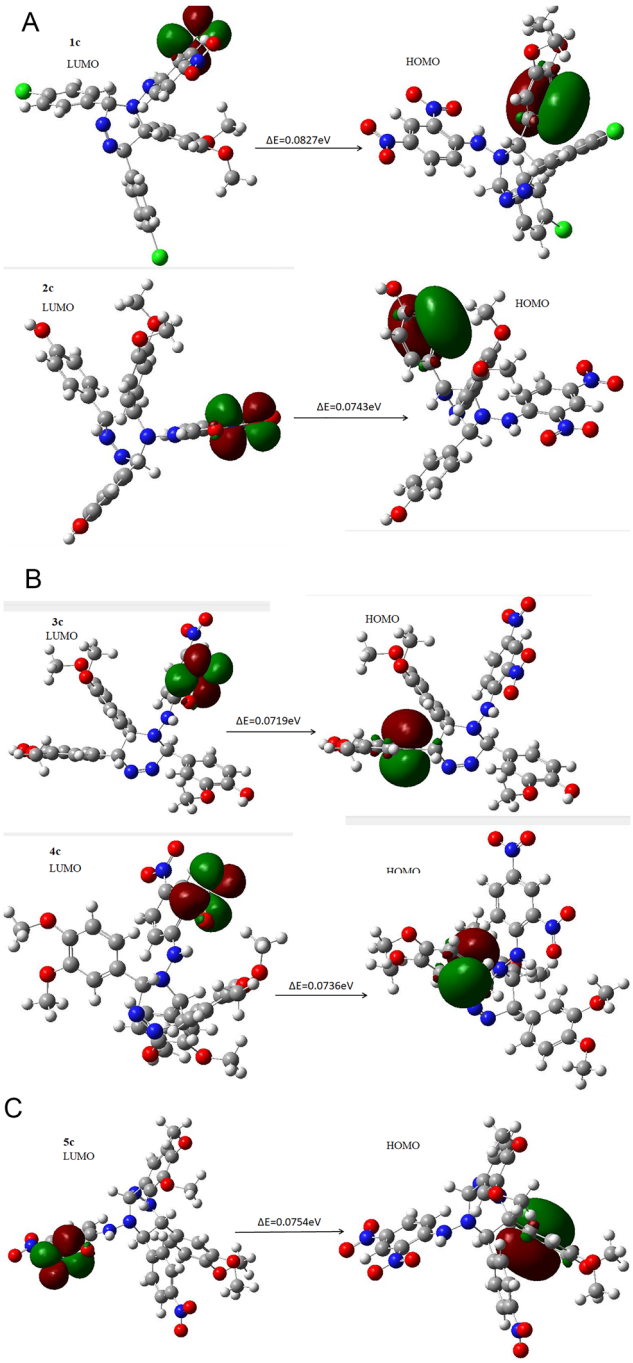

Fig. 8 (A) HOMO–LUMO energy gaps of synthesized compounds **1c** and **2c**. (B) HOMO–LUMO energy gaps of synthesized compounds **3c** and **4c**. (C) HOMO–LUMO energy gaps of synthesized compound **5c** as a dye.

 © 2025 The Author(s). Published by the Royal Society of Chemistry

Open Access Article. Published on 19 August 2025. Downloaded on 3/29/2026 11:26:00 PM.
This article is licensed under a Creative Commons Attribution-NonCommercial 3.0 Unported Licence.

3.4. Optical property analysis by solvatochromism and photochromism

In this research article, the dye compounds (**1c–5c**) showed solvatochromism. These dyes have the capability to form hydrogen bonds with the oxygen atoms (–OH and –OCH_3) of solvents *via* their benzyl, N-atoms of hydrazine, -chloro, -nitro and -methoxy groups. These dyes were dissolved in five different solvents with increasing polarity including ethyl acetate, chloroform, DCM, acetonitrile and DMSO, respectively, as shown in Fig. 5 and 6. With an increase in the polarity of the solvents, the experimental spectra revealed a change in absorbance λ_{max}. The experimental results for dye compound **1c** showed λ_{max} values at 330 nm, 434 nm, 484 nm, 488 nm, and 510 nm, respectively. Also, the theoretical results for this dye showed the maximum wavelength at 340 nm, 342 nm, 381 nm, 385 nm, 388 nm and 392 nm. The experimental results for dye compound **2c** recorded λ_{max} values at 332, 434, 477, and 479 nm. The theoretical results for this dye (**2c**) showed the maximum wavelength at 380 nm and 386 nm. The experimental results for dye compound **3c** recorded λ_{max} values at 332 nm, 434 nm, 497 nm, and 502 nm and the theoretical results for this dye showed the maximum wavelength at 404 nm. The experimental results for dye compound **4c** recorded λ_{max} values at 332 nm, 434 nm, and 508 nm and the theoretical results for this dye showed the maximum wavelength at 412 nm and 416 nm. The experimental results for dye compound **5c** recorded λ_{max} values at 332 nm, 434 nm, and 465 nm and the theoretical results for this dye showed the maximum wavelength at 379 nm, 383 nm and 385 nm.

Comparison of experimental and theoretical λ_{max} values

Dye compound	Experimental λ_{max} (nm)	Theoretical λ_{max} (nm)
1c	330, 434, 484, 488, 510	340, 342, 381, 385, 388, 392
2c	332, 434, 477, 479	380, 386
3c	332, 434, 497, 502	404
4c	332, 434, 508	412, 416
5c	332, 434, 465	379, 383, 385

It is observed that all these dyes revealed the almost same experimental results in different solvents, which nearly match the theoretical results. However, **1c** dye revealed a slight variation in λ_{max} values compared to the other dyes. The change in λ_{max} follows a bathochromic shift.

The solvatochromic properties of the triazine-based dyes (**1c–5c**) were investigated by recording their UV-Vis absorption spectra in solvents of varying polarity including DMSO, acetonitrile, dichloromethane (DCM), chloroform, and ethyl acetate. These dyes feature a central triazine ring substituted with benzene units bearing functional groups such as –NO_2, –Cl, –OH, and –OCH_3, which influence their electronic transitions through their electron-donating or -withdrawing effects. The experimental λ_{max} values demonstrated significant shifts depending on the solvent environment, particularly for the dyes with strong donor–acceptor structures.[42] Notably, compounds **1c** and **3c** exhibited pronounced bathochromic shifts in polar solvents (*e.g.*, DMSO), which is attributed to the enhancement in intramolecular charge transfer (ICT) interactions by polar solvation and hydrogen bonding with groups such as –NO_2 and –OH. In contrast, compounds such as **5c** showed relatively smaller shifts, indicating a weaker solvatochromic response.[43]

These shifts can be explained by the differential stabilization of the ground and excited states in solvents with varying dielectric constants and hydrogen-bonding capabilities. Solvents such as DMSO and acetonitrile, being highly polar and good hydrogen-bond acceptors, preferentially stabilize the excited states, leading to red shifts in the absorption maxima. Chloroform and DCM, with lower polarity and limited hydrogen-bonding capacity, resulted in smaller shifts or even hypsochromic effects. The presence of polar functional groups (*e.g.*, –NO_2 and –OH) in conjugation with the triazine ring facilitated ICT transitions, which are particularly sensitive to the solvent polarity, reinforcing the solvatochromic nature of these dyes.[44,45]

TD-DFT calculations performed using the B3LYP/6-311G(d) method supported the experimental findings by correctly predicting the trend in electronic transitions, although the theoretical λ_{max} values were generally lower due to the use of gas-phase or implicit solvent models.[46,47] Overall, the comparative analysis highlights that the structural features, especially the

Table 2 Quantum parameters of synthesized molecules during optimization

Quantum chemical descriptor	1c	2c	3c	4c	5c
E_{LUMO} (eV)	−0.19589	−0.18960	−0.19046	−0.18913	−0.19618
E_{HOMO} (eV)	−0.27868	−0.26393	−0.26238	−0.26274	−0.27159
Energy gap = $\Delta E = E_{LUMO} - E_{HOMO}$ (eV)	0.08279	0.07433	0.07192	0.07361	0.07541
Ionization potential = IP = $-E_{HOMO}$ (eV)	0.27868	0.26393	0.26238	0.26274	0.27159
Electron affinity = EA = $-E_{LUMO}$ (eV)	0.19589	0.18960	0.19046	0.18913	0.19618
Electronegativity = $x = I + A/2$ (eV)	0.23728	0.22676	0.22642	0.22593	0.23388
Chemical potential = $\mu = -(\mathrm{IP} + \mathrm{EA})/2$ (eV)	−0.23728	−0.22676	−0.22642	−0.22593	−0.23388
Chemical hardness = $\eta = \mathrm{IP} - \mathrm{EA}/2$ (eV)	0.04139	0.03716	0.03596	0.03680	0.03770
Chemical softness = $S = 1/2\eta$ (eV)	12.0787	13.4535	13.9043	13.5851	13.26084
Nucleophilicity index = $N = 1/\omega$ (eV)	1.47041	1.44556	1.40288	1.44201	1.37856
Maximum charge transfer index = $\Delta N_{Max} = -\mu/\eta$ (eV)	5.7322	6.10157	6.29644	6.13870	6.20302
Electrophilicity index = $\omega = \mu 2/2\eta$ (eV)	0.68008	0.69177	0.71281	0.69347	0.72539

Open Access Article. Published on 19 August 2025. Downloaded on 3/29/2026 11:26:00 PM.
This article is licensed under a Creative Commons Attribution-NonCommercial 3.0 Unported Licence.

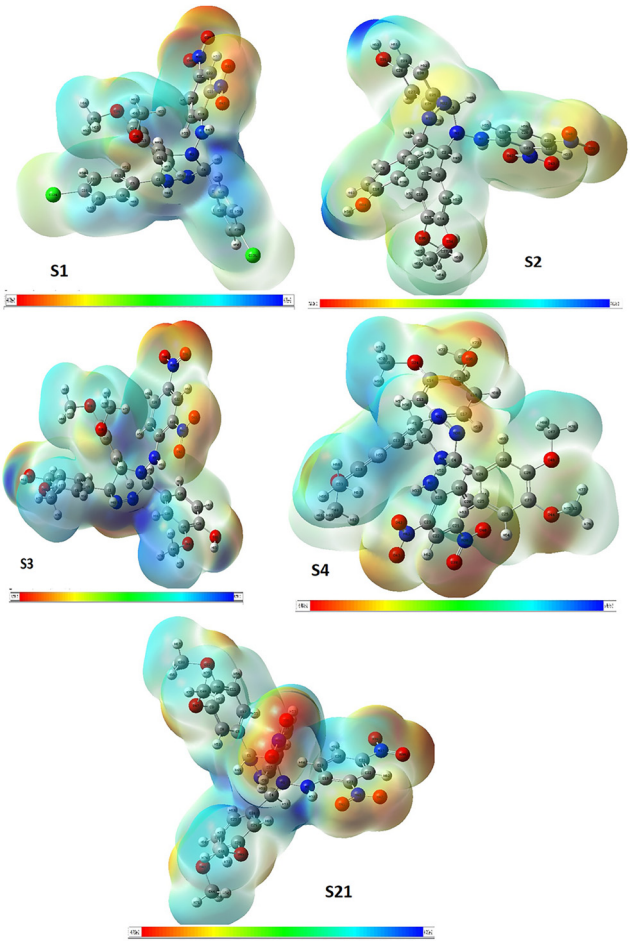

Fig. 9 Molecular electrostatic potential mapping of synthesized molecules **1c–5c** (here **S1** = **1c**, **S2** = **2c**, **S3** = **3c**, **S4** = **4c** and **S21** = **5c**).

distribution of electron-donating and -withdrawing groups, combined with solvent polarity and hydrogen-bonding capability, govern the solvatochromic properties of triazine-based dyes, making them promising candidates for polarity-sensitive applications in the textile and sensing industries.[44]

When exposed to light, a photochromic molecule shifts from a stable form to a new, colored form by rearranging its structure, similar to opening a ring or switching double bonds. This change is temporary and reverses when the light is removed or replaced. In triazine-based compounds with groups such as $-NO_2$, –OH, –Cl, and $-OCH_3$, this light-driven change often happens due to electron movement within their conjugated structure.[48–50]

3.5. Computational analysis of the synthesized compounds

3.5.1. Structure–activity relationship analysis by molecular docking. The chemical structure of a compound decides its biological potential, which depends on its size, alignment of functional groups, configuration, functional group polarity, inter and intra-molecular hydrogen bonding and steric effects. Moreover, these factors can be used to evaluate the function of a compound. The biological potential of the triazine moiety also varies, where the 1,2,4-triazine dye compounds (**1c–5c**) showed excellent docking results with the 4WK1 and 1JIL proteins in the Molegro software. The docking score of these dyes was compared with the reference drug cephalosporin. Dye compound **1c** showed a MolDock score of −156 with the 1JIL protein and eight hydrogen bond interactions with the SER194, GLY49, PRO53, LYS84, LYS231, ASP195, HIS47 and GLY49 amino acids. This dye also showed a MolDock score of −97 with the 4WK1 protein and four hydrogen bond interactions with the GLY47, ALA27, LEU45, and CYC46 amino acids. Dye compound **2c** showed a MolDock score of −174 with the 1JIL protein and six hydrogen bond interactions with the SER194, LYS231 & 234, GLY233, and ASP195 amino acids. This dye also showed a MolDock score of −99 with the 4WK1 protein and three hydrogen bond interactions with the THR28 and ASN24 amino acids. Dye compound **3c** showed a MolDock score of −167 with the 1JIL protein and five hydrogen bond interactions with the VAL224, ILE221, GLY49, THR225, and PHE232 amino acids. This dye also showed a MolDock score of −113 with the 4WK1 protein and nine hydrogen bond interactions with the ARG26, THR28, GLY47, ALA47, and ASN24 amino acids. Dye compound **4c** showed a MolDock score of −163 with the 1JIL protein and eleven hydrogen bond interactions with the VAL224, LYS234 & 231, HIS47, GLY49, LEU223, PHE232, SER194 & 82, and ASP80 amino acids. This dye also showed a MolDock score of −120 with the 4WK1 protein and two hydrogen bond interactions with the

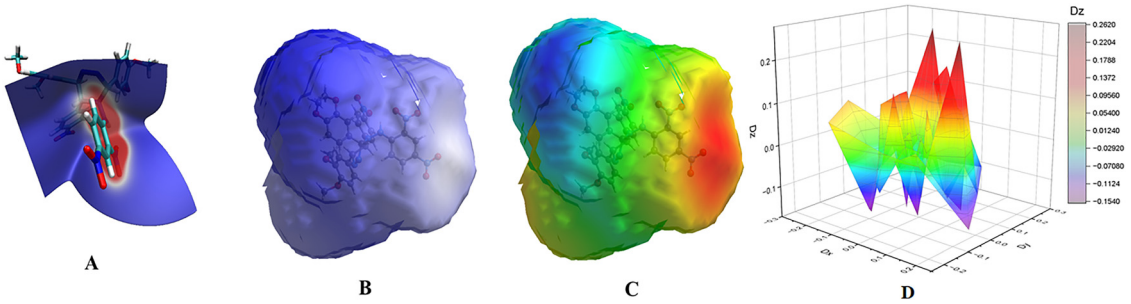

Fig. 10 (A) Molecular structure of **5c** with the surface, showing that their contact is close (red dots represent strong interactions between molecules); (B) Hirshfeld-mapped shape index showing pi–pi stacking interaction using red and blue triangles; (C) Hirshfeld surface and the property of curviness, where flat regions (green) suggest pi–pi stacking and curved (blue) are regions, edges or corners; and (D) **5c** surface area graph visualization for dipole components.

 © 2025 The Author(s). Published by the Royal Society of Chemistry

Open Access Article. Published on 19 August 2025. Downloaded on 3/29/2026 11:26:00 PM.
This article is licensed under a Creative Commons Attribution-NonCommercial 3.0 Unported Licence.

Table 3 Hirshfeld parameters for compound **5c**

Sr no	Atoms	Q–H	S–H	D_x	D_y	D_z	Q-CM5
1	C	0.027317	0	−0.01817	−0.00653	−0.03472	0.032854
2	C	0.030095	0	−0.00413	0.035834	0.017108	0.040383
3	N	−0.08365	0	−0.08629	−0.07496	−0.05558	−0.26342
4	C	0.075828	0	0.019562	−0.0218	−0.0069	0.133647
5	C	−0.01309	0	−0.04068	0.043215	0.001553	−0.01928
6	C	0.007653	0	−0.01522	0.013814	−0.04779	0.001376
7	N	−0.06707	0	0.049719	0.000916	−0.02335	−0.35656
8	C	−0.05688	0	0.01311	0.041223	0.010087	−0.10502
9	C	0.059288	0	0.121286	0.013754	0.051421	0.077278
10	C	0.059909	0	0.098475	−0.0889	−0.01197	0.077881
11	C	−0.05055	0	−0.01641	−0.04383	−0.02956	−0.10125
12	C	−0.05152	0	−0.03578	−0.01106	−0.03015	−0.10275
13	C	−0.03475	0	−0.01164	−0.04754	−0.02174	−0.08788
14	C	−0.02536	0	−0.0012	−0.05711	0.007772	−0.07281
15	C	0.038933	0	0.043772	−0.02013	0.095698	0.090697
16	C	−0.02666	0	0.011386	0.046574	0.027174	−0.07408
17	C	−0.03841	0	−0.00076	0.044689	−0.00588	−0.0902
18	C	0.083202	0	0.034949	0.035359	0.025054	0.152905
19	C	−0.05594	0	0.027148	0.018049	−0.006	−0.10277
20	C	−0.01096	0	−0.00576	−0.02583	−0.05989	−0.05824
21	C	0.027963	0	−0.07432	−0.06137	−0.04058	0.081843
22	C	−0.01591	0	−0.0342	−0.00766	0.028322	−0.05323
23	C	0.025439	0	0.023836	0.051312	0.078835	0.086917
24	C	−0.01849	0	−0.04391	−0.04617	−0.00869	−0.02067
25	C	−0.05478	0	−0.0107	−0.00839	−0.04978	−0.1055
26	C	−0.04801	0	0.021233	0.019456	−0.05068	−0.09871
27	C	0.060044	0	0.060031	0.118726	0.0168	0.078001
28	C	0.0593	0	0.018451	0.060237	0.115596	0.077369
29	C	−0.06049	0	−0.02374	−0.0093	0.030086	−0.10737
30	N	−0.07901	0	0.147909	−0.0161	0.260939	−0.16743
31	N	−0.06535	0	−0.05242	0.120377	0.256384	−0.15327
32	O	−0.17605	0	0.042365	0.240954	−0.09335	−0.25954
33	C	−0.00874	0	−0.0307	−0.02302	0.022426	−0.13386
34	N	0.210932	0	0.004918	−0.00277	0.014291	0.05513
35	O	−0.19733	0	−0.07253	−0.12943	−0.13691	−0.16274
36	O	−0.19792	0	−0.04317	0.179401	−0.08186	−0.16334
37	N	0.207814	0	−0.0135	−0.00975	−0.00517	0.050951
38	O	−0.19662	0	0.163641	0.056014	−0.09838	−0.16188
39	O	−0.20154	0	0.022019	0.092415	0.178644	−0.1672
40	N	0.206575	0	−0.00024	0.008755	0.02084	0.048746
41	O	−0.19315	0	−0.07553	−0.11589	−0.1483	−0.17233
42	O	−0.18036	0	0.129965	0.025612	−0.13706	−0.14669
43	O	−0.17482	0	−0.2464	−0.02752	0.080128	−0.25867
44	C	−0.00781	0	0.033675	−0.02364	−0.01637	−0.13302
45	O	−0.17538	0	0.209667	−0.0439	−0.14862	−0.25877
46	C	−0.00905	0	−0.04388	−0.00017	−0.00075	−0.1342
47	O	−0.17638	0	−0.1448	−0.20646	0.071031	−0.25984
48	C	−0.00924	0	0.002345	0.033111	−0.02927	−0.13438
49	H	0.049464	0	0.070453	0.104097	0.028301	0.126076
50	H	0.031063	0	−0.04447	−0.10618	−0.03305	0.107905
51	H	0.057975	0	−0.13594	0.044541	−0.02766	0.143815
52	H	0.113754	0	0.042164	0.084022	0.11036	0.340034
53	H	0.05339	0	0.037519	0.126095	0.075303	0.114135
54	H	0.059772	0	−0.03354	−0.12751	−0.09163	0.119057
55	H	0.049421	0	−0.12212	−0.03963	−0.07403	0.110781
56	H	0.058233	0	−0.04926	−0.12721	−0.07381	0.115936
57	H	0.064503	0	0.00037	−0.15999	0.017727	0.128758
58	H	0.063169	0	0.037646	0.138784	0.067742	0.127492
59	H	0.050292	0	−0.00363	0.13117	−0.01852	0.112007
60	H	0.047972	0	0.081717	0.009735	−0.09812	0.119812
61	H	0.070842	0	0.031766	−0.04314	−0.1536	0.135172
62	H	0.068128	0	−0.11546	−0.03155	0.088247	0.141911
63	H	0.053153	0	−0.0168	−0.03418	−0.14522	0.115898
64	H	0.061761	0	0.044479	0.07408	−0.13674	0.121058
65	H	0.050163	0	−0.04656	−0.05453	0.127677	0.115768
66	H	0.043082	0	0.092907	0.092167	0.028115	0.106073
67	H	0.056481	0	0.097765	−0.11918	−0.00751	0.11658
68	H	0.044696	0	−0.01765	0.031004	−0.13763	0.103309
69	H	0.045227	0	−0.1097	0.040125	−0.08173	0.103853
70	H	0.043882	0	−0.05872	0.015738	0.120369	0.10657

Open Access Article. Published on 19 August 2025. Downloaded on 3/29/2026 11:26:00 PM.
This article is licensed under a Creative Commons Attribution-NonCommercial 3.0 Unported Licence.

Table 3 (*continued*)

Sr no	Atoms	Q–H	S–H	D_x	D_y	D_z	Q-CM5
71	H	0.05738	0	0.083736	0.130297	0.00491	0.117483
72	H	0.057944	0	−0.00057	0.061839	0.143041	0.118097
73	H	0.042382	0	0.081584	−0.11158	0.018543	0.100943
74	H	0.043426	0	0.094383	0.082242	−0.04704	0.106999
75	H	0.043136	0	0.024724	−0.13171	−0.00606	0.106248
76	H	0.056943	0	0.139151	0.037983	0.056421	0.11705
77	H	0.042874	0	−0.07202	−0.00153	0.114314	0.101612

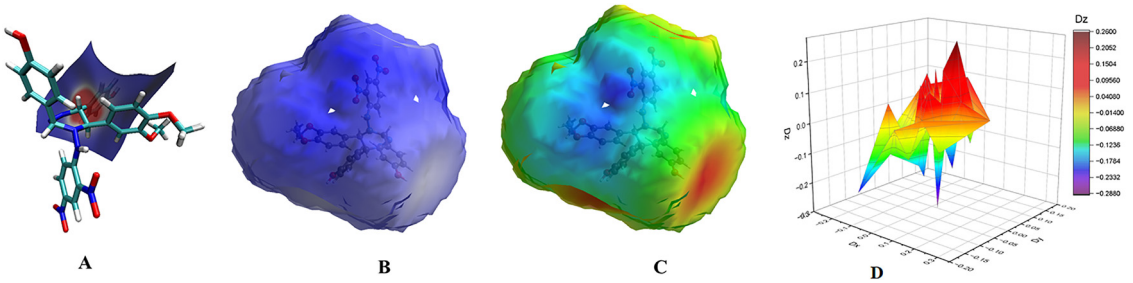

Fig. 11 (A) Molecular structure of **2c** with the surface, showing that their contact is close (red dots represent strong interactions between molecules; (B) Hirshfeld-mapped shape index showing pi–pi stacking interaction using red and blue triangles; (C) Hirshfeld surface and the property of curviness, where flat regions (green) suggest pi–pi stacking and curved (blue) are regions, edges or corners; and (D) **2c** surface area graph visualization for dipole components.

HIS107 and GLY47 amino acids. The fifth novel dye compound **5c** showed a MolDock score of −141 with the 1JIL protein and twelve hydrogen bond interactions with the THR42, HIS47 & 50, LYS84 & 234, ASP80 & 195, GLN196, SER82, and GLY49 amino acids. This dye also showed a MolDock score of −135 with the 4WK1 protein and no hydrogen bond interactions with amino acids. These novels 1,2,4-triazine dyes showed the best MolDock score with both proteins compared to the reference drug cephalosporin. To present more detailed results for understanding, all the 3D and 2D interactions of the synthesized molecules with both proteins are displayed in Fig. 7a and b and Fig. S7–S14 (SI) and Table S1 (SI).

The molecular docking results of the five 1,2,4-triazine-based dye compounds (**1c–5c**) against the biological targets 1JIL and 4WK1 reveal distinct variations in binding affinities and interaction patterns. Among them, compound **4c** stood out with the strong MolDock score of −120 against 4WK1 and formed two hydrogen bonds, suggesting a highly stable and favorable interaction with the active site. This was followed by compound **1c**, which showed a score of −97 with 4WK1 and −156 with 1JIL, establishing its dual-target binding ability with eight hydrogen bonds in 1JIL and four in 4WK1. Compound **2c** also showed promising docking, scoring −99 with 4WK1 and −174 with 1JIL, and forming a total of nine hydrogen bonds across both proteins, reflecting its good binding potential and interaction diversity.[51,52]

In contrast, compound **3c** demonstrated moderate binding affinity with scores of −113 (4WK1) and −167 (1JIL), with more hydrogen bonds compared to the other compounds, indicating its relatively greater binding stability. Compound **5c**, while showing the lowest docking score with 1JIL (−141), formed the highest number of hydrogen bonds (12) with this target, suggesting its strong surface-level interactions despite weaker overall binding energy. However, its performance with 4WK1 was better (−135) with no hydrogen bonds, positioning it above compound **3c** in terms of overall affinity. These comparative results indicate that compounds **4c** and **1c** have the most favorable profiles for biological activity, while **2c** and **5c** also show notable interaction capabilities, warranting further biological validation.[53–55]

3.5.2. Theoretical calculation by DFT/TD-DFT studies. The configuration of the target compounds (**1c–5c**) was optimized by density functional theory to further acquire their durable atomic alignment. The HOMO & LUMO orbitals of the compounds were observed by DFT analysis, which presented the value of stability, energy gap, distribution of energy around the structure, and reactivity of the compounds.[56] The HOMO & LUMO parameters are utilized to estimate the molecular reactivity and chemical reactivity descriptors (Fig. 8a–c). The energy of the lowest unoccupied molecular orbital (LUMO) was calculated to be −0.195.89, −0.18960, −0.19046, −0.18913, and 0.19618 for dye compounds **1c**, **2c**, **3c**, **4c**, and **5c**, respectively. The energy of the highest occupied molecular orbital (HOMO) was calculated to be 0.27868, −0.26393, −0.26238, −0.26274, and −0.27159 for dye compounds **1c–5c**, respectively. The energy gap of the 1,2,4-triazine dye compounds was evaluated to be 0.08279 for **1c**, 0.07433 for **2c**, 0.07192 for **3c**, 0.07361 for **4c** and 0.07541 for **5c**. The other values of chemical reactivity descriptors are revealed in Table 2. The stability and reactivity of the dye compounds were studied based on their molecular

 © 2025 The Author(s). Published by the Royal Society of Chemistry

Open Access Article. Published on 19 August 2025. Downloaded on 3/29/2026 11:26:00 PM.
This article is licensed under a Creative Commons Attribution-NonCommercial 3.0 Unported Licence.

Table 4 Hirshfeld parameters for compound **2c**

Sr no	Atoms	Q–H	S–H	D_x	D_y	D_z	Q-CM5
1	C	0.025677	0	0.020024	0.011452	0.032209	0.031094
2	C	0.029307	0	0.002319	0.02655	−0.03044	0.039057
3	N	−0.08466	0	0.092995	−0.03346	0.075023	−0.2644
4	C	0.073637	0	−0.01964	−0.01911	0.016505	0.13173
5	C	−0.01796	0	0.039808	0.035251	−0.02163	−0.02444
6	C	−0.01549	0	0.01392	0.037306	0.037416	−0.0214
7	N	−0.06343	0	−0.05201	0.001817	0.022803	−0.35336
8	C	−0.04438	0	−0.02034	0.023841	−0.0425	−0.0976
9	C	−0.07449	0	−0.04334	−0.00518	−0.01875	−0.12648
10	C	0.074529	0	−0.09254	−0.08264	0.064222	0.085068
11	C	−0.05446	0	0.005756	−0.02322	0.047914	−0.10537
12	C	−0.04108	0	0.04066	0.008795	0.027555	−0.09232
13	C	−0.05452	0	0.021605	−0.02028	0.031105	−0.10273
14	C	0.060138	0	0.012764	−0.13182	0.010666	0.078105
15	C	0.060108	0	−0.04905	−0.08611	−0.08826	0.078125
16	C	−0.05117	0	−0.03112	0.023225	−0.03825	−0.10192
17	C	−0.05453	0	−0.01129	0.042682	−0.00982	−0.10662
18	C	0.085212	0	−0.03862	0.014614	−0.03462	0.155404
19	C	−0.0547	0	−0.03118	0.015313	−0.00246	−0.10154
20	C	−0.01198	0	0.009607	0.003399	0.064066	−0.05926
21	C	0.026875	0	0.079355	−0.03053	0.059592	0.080939
22	C	−0.01663	0	0.032754	−0.01806	−0.02363	−0.05394
23	C	0.025322	0	−0.0319	0.006235	−0.09079	0.087011
24	O	−0.21928	0	−0.07041	0.1282	−0.22853	−0.41411
25	C	−0.02566	0	0.044594	−0.03468	0.025077	−0.02804
26	C	−0.04685	0	0.012847	−0.03251	−0.0307	−0.09859
27	C	−0.05501	0	−0.01361	0.002142	−0.05113	−0.10596
28	C	0.075929	0	−0.07052	0.103297	−0.06436	0.086577
29	C	−0.07124	0	−0.01243	0.042012	0.023581	−0.12314
30	C	−0.04721	0	0.019675	0.014887	0.04889	−0.09816
31	O	−0.21683	0	0.069431	0.033511	0.259589	−0.41176
32	N	−0.08396	0	−0.14365	−0.1509	−0.22133	−0.171
33	N	−0.06941	0	0.047072	−0.01452	−0.28755	−0.15659
34	O	−0.17557	0	−0.24055	0.102291	0.00303	−0.25923
35	C	−0.00915	0	0.043636	0.011882	−0.00612	−0.1342
36	O	−0.17747	0	0.260326	0.001544	0.038427	−0.26062
37	C	−0.00891	0	−0.03556	0.019487	0.015433	−0.13403
38	N	0.206896	0	0.014203	−0.00573	0.008363	0.049947
39	O	−0.19971	0	−0.16741	0.083162	0.072526	−0.16502
40	O	−0.20397	0	−0.03566	−0.00278	−0.20045	−0.16969
41	N	0.205616	0	−0.00203	−0.0024	−0.02191	0.047728
42	O	−0.19525	0	0.089771	−0.02908	0.181141	−0.17428
43	O	−0.18525	0	−0.1308	0.07593	0.120118	−0.15168
44	H	0.047796	0	−0.07698	0.072604	−0.07111	0.12443
45	H	0.028905	0	0.05315	−0.07365	0.076516	0.105514
46	H	0.054409	0	0.130131	0.058785	0.000655	0.140166
47	H	0.113844	0	−0.05385	0.016857	−0.13291	0.340099
48	H	0.050253	0	−0.05378	0.068985	−0.11993	0.107865
49	H	0.049099	0	−0.13837	−0.01759	−0.06854	0.107078
50	H	0.060068	0	0.042948	−0.06964	0.139758	0.119523
51	H	0.050564	0	0.12558	0.007132	0.076849	0.111868
52	H	0.055263	0	0.073636	−0.06403	0.119337	0.115867
53	H	0.058763	0	−0.07526	0.063715	−0.12558	0.118027
54	H	0.044584	0	−0.02774	0.126734	−0.03238	0.104994
55	H	0.048918	0	−0.08179	0.047434	0.088682	0.120021
56	H	0.070013	0	−0.0245	0.02927	0.157623	0.134342
57	H	0.067174	0	0.115347	−0.05981	−0.0709	0.140967
58	H	0.189395	0	−0.18324	−0.02908	−0.07677	0.358717
59	H	0.046811	0	0.033617	−0.1019	−0.09295	0.109847
60	H	0.060517	0	−0.03722	−0.01997	−0.15692	0.119974
61	H	0.051231	0	−0.03565	0.127335	0.084057	0.109242
62	H	0.054024	0	0.033572	0.041507	0.139512	0.116177
63	H	0.191368	0	−0.05147	0.169821	0.095794	0.360667
64	H	0.056326	0	0.036299	−0.14881	0.017553	0.116429
65	H	0.044422	0	−0.06756	0.024631	0.119937	0.103078
66	H	0.042546	0	−0.10618	−0.02073	−0.07868	0.105271
67	H	0.05577	0	−0.07649	−0.08839	−0.09986	0.115861
68	H	0.045398	0	0.089232	0.070485	−0.08661	0.104019
69	H	0.043074	0	0.085067	−0.09545	0.039326	0.106253

Open Access Article. Published on 19 August 2025. Downloaded on 3/29/2026 11:26:00 PM.
This article is licensed under a Creative Commons Attribution-NonCommercial 3.0 Unported Licence.

electrostatic potential maps and scale through DFT. The MEP study indicates the nucleophilic and electrophilic sites in a structure.[57] Alternatively, in the MEP scale, blue color indicates the maximum electrophilicity, red indicates maximum nucleophilicity, green for neutral, yellow for minimum nucleophilicity and sky blue for minimum electrophilicity.[58]

Density functional theory calculations for the five 1,2,4-triazine-based dye compounds (**1c–5c**) reveal important trends in their electronic structures related to stability and chemical reactivity. Compound **1c** shows the highest HOMO energy (0.27868 eV) and the largest HOMO–LUMO gap (0.08279 eV), indicating it is the most electronically stable and least reactive among the series. In contrast, compound **3c** has the smallest energy gap (0.07192 eV), suggesting its greater chemical reactivity and lower kinetic stability due to easier electron excitation.[59]

The moderate energy gaps observed in compounds **2c**, **4c**, and **5c** place them between these two extremes, reflecting their balanced stability and reactivity. The variation in energy gaps across the series can be attributed to the different electron-donating and electron-withdrawing substituents ($-NO_2$, –Cl, –OH, $-OCH_3$) attached to the triazine core and aromatic rings, which modulate the distribution of the frontier molecular orbitals and influence the electron density delocalization. Thus, from a theoretical standpoint, the compounds with lower HOMO–LUMO gaps (*e.g.*, **3c** and **4c**) are predicted to be more reactive and less stable, while those with higher gaps (*e.g.*, **1c**) offer enhanced stability, which is a key consideration for their practical applications and durability.[24,60,61]

In the current research, the molecular electrostatic potential maps of all the dyes (**1c–5c**) showed that the chloro, hydroxy and nitro groups of 2,4-dinitrophenyl hydrazine occupied the less nucleophilic region. Methoxy groups and triazine core were found in the neutral region (Fig. 9). However, in dye **5c**, 4-nitrobenzene revealed the maximum nucleophilicity. According to the comparison of the theoretical results with the experimental results, it is clear that these groups lie in the less nucleophilic region.[62]

3.5.3. Dye compound surface analysis through Hirshfeld parameters

*3.5.3.1. Hirshfeld parameters of compound **5c**.* Key descriptive terms, including Q–H (a partial atomic charge *via* Hirshfeld analysis of the overall population), S–H (perhaps spin and symmetry-related variable, all zero here), oriented elements that constitute a dipole moment (D_x, D_y, and D_z), as well as Q-CM5 (charge about CM5 method), were given through the Hirshfeld analysis of compound **5c**, which offers an extensive quantum chemical study of 77 atoms, such as carbon (C), nitrogen (N), oxygen (O), and hydrogen (H). The various atoms have different electron densities with bonding environments, and these were expressed in their Q–H values. Among the electronegative atoms, both nitrogen and oxygen have much larger electron affinities with higher negative values (Fig. 10). The CM5 charges contribute fine-tuned distributions of charging that are suitable for force-field generation or electrostatic potential mapping, although the dipole components (D_x, D_y, and D_z) give data concerning the arrangement of molecule polarity, as shown in Table 3.

*3.5.3.2. Hirshfeld parameters of compound **2c**.* The dataset for **2c** contains extensive atomic-level parameters for a compound composed of 69 atomic particles, including hydrogen, oxygen, nitrogen, and carbon. Regardless of their powerful electronegativity and frequent occurrence in polar functional groups such carbonyls and amides, oxygen and nitrogen atoms carry considerable negative charges based on their partial charges estimated using quantum chemical reactions methods (Fig. 11). Depending on their immediate chemical environment, carbon atoms exhibit a wide range of partial charges, whereas hydrogen atoms predominantly carry positive charges, which is associated with their electron-deficient characteristic. With atoms diffused along all axes, the spatial characteristics suggest a non-planar peptide with a significant three-dimensional architecture. Notably, the existence of highly charged hydrogen atoms including strongly charged oxygen, nitrogen, and both indicates the potential of polar interactions as well as intra-molecular bonds of hydrogen. This molecule possesses substantial dipole moments as well as the capacity to interact aggressively with solvents and biological targets, depending on its charge separation or geometry (Table 4).

*3.5.3.1. Hirshfeld parameters of compound **1c**.* The dataset showed complete atomic-level details for molecule **1c**, which is

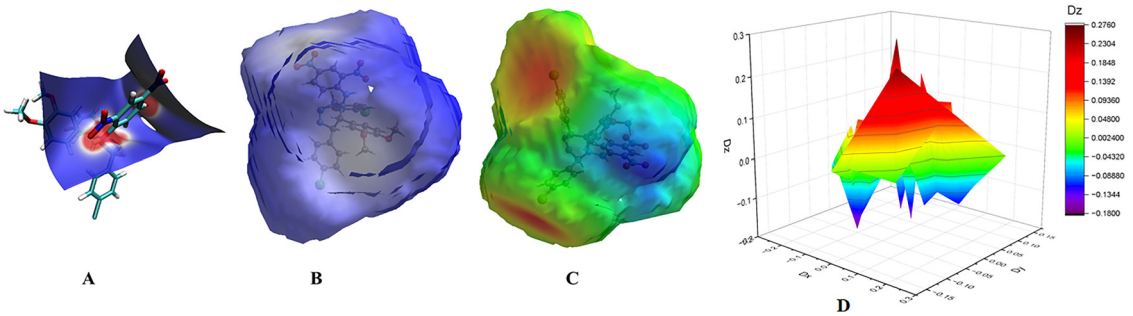

Fig. 12 (A) Molecular structure of **1c** with the surface, showing that their contact is close (red dots represent strong interactions between molecules); (B) Hirshfeld-mapped shape index showing pi–pi stacking interaction using red and blue triangles; (C) Hirshfeld surface and the property of curviness, where flat regions (green) suggest pi–pi stacking and curved (blue) are regions, edges or corners; and (D) **1c** surface area graph visualization for dipole components.

 © 2025 The Author(s). Published by the Royal Society of Chemistry

Open Access Article. Published on 19 August 2025. Downloaded on 3/29/2026 11:26:00 PM.
This article is licensed under a Creative Commons Attribution-NonCommercial 3.0 Unported Licence.

Table 5 Hirshfeld parameters of compound **1c**

Sr no	Atoms	Q–H	S–H	D_x	D_y	D_z	Q-CM5
1	C	0.027149	0	−0.01412	0.004325	−0.03574	0.032885
2	C	0.029958	0	−0.00535	0.031986	0.024097	0.039549
3	N	−0.08464	0	−0.08619	−0.05171	−0.07482	−0.26438
4	C	0.074903	0	0.021682	−0.01888	−0.01109	0.133225
5	C	−0.00442	0	−0.04002	0.039751	0.013403	−0.01088
6	C	−0.01745	0	−0.01162	0.029398	−0.0446	−0.02342
7	N	−0.06541	0	0.054622	−0.00355	−0.01934	−0.3551
8	C	−0.03821	0	0.018312	0.028781	0.039177	−0.09147
9	C	−0.04443	0	0.043979	0.009562	0.040208	−0.09726
10	C	0.036825	0	0.075801	−0.06828	−0.03143	0.029694
11	C	−0.04384	0	−0.02189	−0.02148	−0.05221	−0.09656
12	C	−0.03732	0	−0.034	0.001059	−0.03605	−0.08855
13	C	−0.0548	0	−0.01905	−0.02739	−0.0276	−0.10301
14	C	0.061657	0	−0.00773	−0.1316	0.013301	0.07974
15	C	0.061926	0	0.043995	−0.06664	0.106122	0.080005
16	C	−0.05	0	0.027565	0.030757	0.036549	−0.10077
17	C	−0.05569	0	0.009878	0.043843	0.003221	−0.1078
18	C	0.084416	0	0.035563	0.022742	0.034893	0.154327
19	C	−0.05554	0	0.029467	0.016607	0.000689	−0.10242
20	C	−0.01111	0	−0.00427	−0.00868	−0.06455	−0.05838
21	C	0.02793	0	−0.07414	−0.04449	−0.05827	0.081858
22	C	−0.01561	0	−0.03467	−0.01481	0.024293	−0.05292
23	C	0.025973	0	0.023773	0.023811	0.090722	0.087556
24	Cl	−0.09803	0	−0.08257	0.078395	0.031896	−0.10023
25	C	−0.01216	0	−0.04087	−0.04015	−0.0236	−0.01453
26	C	−0.0432	0	−0.0129	−0.02318	0.038418	−0.09501
27	C	−0.04414	0	−0.00012	−0.00854	0.058883	−0.0969
28	C	0.037471	0	0.045907	0.089014	0.037352	0.030349
29	C	−0.04118	0	0.008903	0.035592	−0.05038	−0.0939
30	C	−0.04087	0	−0.01511	0.00816	−0.05204	−0.09182
31	Cl	−0.09191	0	−0.0502	−0.09189	−0.04075	−0.09411
32	N	−0.07968	0	0.125696	−0.10107	0.253725	−0.16675
33	N	−0.06598	0	−0.07002	0.034146	0.275664	−0.15413
34	O	−0.17509	0	0.237046	0.109283	0.001715	−0.25864
35	C	−0.00813	0	−0.04322	0.009968	−0.00034	−0.13333
36	O	−0.17565	0	−0.25449	−0.01718	−0.05808	−0.25903
37	C	−0.00788	0	0.036668	0.017299	−0.01541	−0.13308
38	N	0.207698	0	−0.01349	−0.00765	−0.00805	0.050796
39	O	−0.19714	0	0.169489	0.074201	−0.07398	−0.16241
40	O	−0.20199	0	0.018664	0.036711	0.198368	−0.16767
41	N	0.2065	0	0.000058	0.001675	0.022072	0.048637
42	O	−0.19475	0	−0.07425	−0.06604	−0.17835	−0.1739
43	O	−0.18205	0	0.136646	0.057392	−0.12138	−0.14839
44	H	0.049795	0	0.070669	0.089218	0.062541	0.126202
45	H	0.029793	0	−0.04535	−0.08933	−0.06536	0.106357
46	H	0.057569	0	−0.13299	0.052456	−0.02298	0.143393
47	H	0.113603	0	0.042692	0.042195	0.131007	0.33996
48	H	0.053605	0	0.042128	0.086316	0.114377	0.111406
49	H	0.062134	0	0.129675	0.000462	0.095648	0.119436
50	H	0.062193	0	−0.03789	−0.0814	−0.13377	0.119498
51	H	0.053878	0	−0.11585	−0.00641	−0.09394	0.115816
52	H	0.055546	0	−0.06134	−0.08824	−0.11115	0.116163
53	H	0.059821	0	0.062542	0.088623	0.118169	0.11911
54	H	0.043757	0	0.021169	0.131925	0.011057	0.104146
55	H	0.048244	0	0.087219	0.0339	−0.0901	0.119248
56	H	0.070572	0	0.036107	0.000506	−0.15838	0.134909
57	H	0.067994	0	−0.11933	−0.05072	0.072477	0.141759
58	H	0.049881	0	−0.03761	−0.08518	0.109737	0.112978
59	H	0.06252	0	0.018814	−0.00091	0.160334	0.119812
60	H	0.064209	0	0.034952	0.109348	−0.11476	0.121528
61	H	0.058052	0	−0.02389	0.013989	−0.14964	0.120236
62	H	0.045375	0	0.078706	0.004554	−0.11464	0.104028
63	H	0.043355	0	0.098712	−0.00214	0.09111	0.106273
64	H	0.057374	0	−0.031	−0.15171	0.007436	0.117491
65	H	0.043741	0	−0.07938	−0.10486	−0.02786	0.106786
66	H	0.057042	0	0.070758	−0.06588	0.120793	0.117157
67	H	0.045843	0	−0.09791	0.081668	0.065325	0.104468

Open Access Article. Published on 19 August 2025. Downloaded on 3/29/2026 11:26:00 PM.
This article is licensed under a Creative Commons Attribution-NonCommercial 3.0 Unported Licence.

composed of 67 atoms, including hydrogen (H), carbon (C), nitrogen (N), oxygen (O), and chlorine (Cl). The fractional atomic charge (Q–H), spinning charge (S–H, all of which are zero here), spatial movement components across the y, z, and x axes (D_x, D_y, and D_z) (Fig. 12), and the CM5 partial charge (Q-CM5) are some of the many calculated characteristics used to characterize a single atom. Due to their many bonding situations inside molecule **1c**, carbon atoms manifest a range of a partial charges, most of which are small and either positive or negative. Importantly, carbons that are closer to electronegative atoms usually possess larger negative values, reflecting localized modifications in the electron density. Considering their increased electronegativity and involvement in electron-withdrawing groups as well as lone pair regions, nitrogen atoms have considerably negative partial charges.

Considering the Q–H values, which are range from approximately −0.18 to −0.20, the oxygen atoms show the most negative charges, emphasizing their strong electronegativity-associated impact on the polarity of molecules. With halogen substituents, chlorine atoms show negative partial charges in the range of −0.09 to −0.10, which makes them compatible with their electron-withdrawing properties. The positive partial charges that hydrogen atoms carry are homogeneous but are in the range of around 0.04 to 0.11, which are typical of hydrogen involved in polar bonds or linked to electronegative atoms (Table 5).

*3.5.3.1. Hirshfeld parameters of compound **3c**.* Significant details regarding the electronic structure of molecule **3c** can be obtained from its CM5 atomic charge or dipole component analysis. Particularly, in combination with or close to electronegative atoms, carbon atoms exhibit an extensive spectrum of partial charges, spanning slightly negative to moderately positive (about −0.13 to +0.16), indicating their varying chemical the surroundings. With values such −0.269 and −0.3488, nitrogen atoms show noticeably negative charges, which are in line with their elevated electronegativity along with electron-donating lone pairs. Because oxygen atoms are involved in polar bonds and possible hydrogen bonding interactions, it is not surprising that they have the highest negative CM5 charges in the system, with values as low as −0.412. In general, hydrogen atoms possess positive charges of around +0.10 to +0.36, particularly when they are linked to negatively charged centers such oxygen and nitrogen (Fig. 13).

A few types of atoms, particularly nitrogen and oxygen atoms, showed substantial vector components with reference to dipole contributions. For example, O24 and O31 have high D_y and D_x numbers, respectively, and make a substantial contribution to the molecule dipole moments. These additions draw attention to regions of the molecule that show high local polarity. When hydrogen atoms form polar relationships, such as those involving charged oxygen or nitrogen atoms, they additionally demonstrate significant dipole components. Overall, the data show a dispersed pattern of electronic density, resulting in concentrated polarity areas surrounding the electronegative atoms as well as the dipoles that go with them. Understanding the reactivity, potential interactions sites, and behavior of this molecule in numerous chemical or biological settings requires this electronic asymmetry (Table 6).

*3.5.3.4. Hirshfeld parameters of compound **4c**.* A strongly polarized electronic structure featuring significant separation of charges across molecule **4c** was shown by its CM5 charge as well as dipole moment data. Due to their electronegativity as well as contributions to polar functional groups, oxygen and nitrogen atoms have the greatest number of unfavorable CM5 charges (*e.g.*, O36 at −0.25574, N7 at −0.35596). Conversely, carbon atoms have an extensive variety of charges based on their connecting environment, which range from optimistic (C18 at +0.16367) to negative (C13 at −0.12994). Small positive charges usually are carried by hydrogen atoms; the greatest values are observed when they are connected to electronegative atoms (for example, H53 at +0.32766). The molecule is crucial both chemically and biologically because of these charge and dipole patterns (Fig. 14), which point to areas of high reactance, especially within the nitrogen as well as oxygen centers, and significant opportunities for intermolecular interactions such as hydrogen bonding (Table 7).

3.5.4. Dye compound surface analysis through topological studies

3.5.4.1. LOL/ELF analysis. Localized orbital locator (LOL) and electron localization function (ELF) analysis gives information about a molecular surface to identify electron pairs based on a projection map. In the projection map, narrow and broad peaks

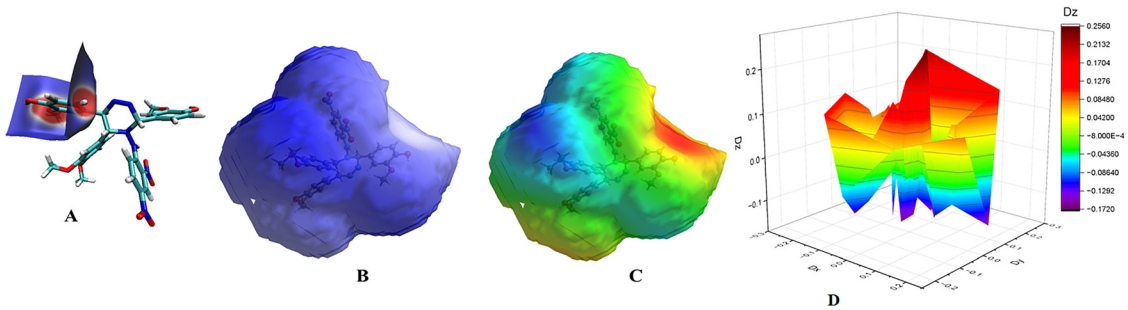

Fig. 13 (A) Molecular structure of **3c** with the surface, showing that their contact is close (red dots represent strong interactions between molecules); (B) Hirshfeld-mapped shape index showing pi–pi stacking interaction using red and blue triangles; (C) Hirshfeld surface and the property of curviness, where flat regions (green) suggest pi–pi stacking and curved (blue) are regions, edges or corners; and (D) surface area graph visualization for dipole components of compound **3c**.

 © 2025 The Author(s). Published by the Royal Society of Chemistry

Open Access Article. Published on 19 August 2025. Downloaded on 3/29/2026 11:26:00 PM.
This article is licensed under a Creative Commons Attribution-NonCommercial 3.0 Unported Licence.

Table 6 Hirshfeld parameters of compound **3c**

Sr no	Atoms	Q–H	S–H	D_x	D_y	D_z	Q-CM5
1	C	0.024455	0	0.019585	−0.02149	−0.03644	0.029258
2	C	0.02401	0	0.032397	−0.00535	0.021157	0.032254
3	N	−0.09285	0	0.03365	0.128651	−0.09483	−0.26906
4	C	0.068778	0	−0.04748	−0.01018	0.012552	0.129855
5	C	−0.01842	0	0.053859	−0.0081	0.018865	−0.02472
6	C	−0.01268	0	0.020432	−0.04005	−0.03752	−0.01811
7	N	−0.05891	0	−0.02708	−0.03942	−0.02611	−0.3488
8	C	−0.07352	0	0.006377	−0.007	0.032962	−0.12307
9	C	0.04821	0	−0.10275	−0.00229	0.082819	0.065665
10	C	0.066073	0	−0.12836	0.004297	−0.02377	0.082062
11	C	−0.05482	0	−0.01454	−0.00341	−0.05529	−0.10557
12	C	−0.05502	0	0.023074	−0.00879	−0.04305	−0.10604
13	C	−0.05346	0	−0.00704	0.015919	−0.03994	−0.10174
14	C	0.060012	0	−0.07094	0.108323	−0.03129	0.07803
15	C	0.058693	0	−0.05791	0.077217	0.090862	0.076726
16	C	−0.05215	0	0.00588	−0.01744	0.05146	−0.10291
17	C	−0.0547	0	0.023668	−0.03903	0.017991	−0.10618
18	C	0.088455	0	−0.00673	−0.03909	0.0286	0.159788
19	C	−0.05369	0	−0.01783	−0.03492	0.001068	−0.10114
20	C	−0.0131	0	−0.01413	0.0201	−0.05931	−0.0604
21	C	0.026519	0	0.022038	0.085543	−0.05306	0.080726
22	C	−0.01578	0	0.023642	0.028509	0.02381	−0.05307
23	C	0.026518	0	0.009532	−0.04528	0.08397	0.088408
24	O	−0.22113	0	0.075654	−0.0209	0.25576	−0.41236
25	C	−0.02131	0	−0.05258	0.012349	−0.02488	−0.02127
26	C	−0.05274	0	0.017733	0.012415	−0.05255	−0.10522
27	C	−0.05261	0	0.049819	−0.00089	−0.02913	−0.10338
28	C	0.071711	0	0.094497	−0.06436	0.062229	0.087887
29	C	0.052946	0	0.003941	−0.06842	0.113133	0.070702
30	C	−0.07431	0	−0.0264	−0.00447	0.017502	−0.1207
31	O	−0.2168	0	−0.23744	−0.00047	0.120074	−0.40818
32	N	−0.08119	0	−0.11643	0.207803	0.210698	−0.1609
33	N	−0.07733	0	0.120046	0.245535	0.136176	−0.16134
34	O	−0.17483	0	−0.12119	−0.19926	0.116304	−0.25845
35	C	−0.00864	0	0.040851	0.015701	−0.0145	−0.13374
36	O	−0.17791	0	0.185134	0.114444	−0.14862	−0.26106
37	C	−0.00823	0	−0.01992	−0.03756	0.004909	−0.13342
38	N	0.206504	0	0.004625	0.015293	−0.00725	0.049427
39	O	−0.20027	0	−0.10568	−0.15302	−0.07572	−0.16559
40	O	−0.20544	0	0.039657	−0.0637	0.190066	−0.17125
41	N	0.205674	0	0.005344	−0.00591	0.020167	0.047551
42	O	−0.19653	0	−0.00596	0.117731	−0.17047	−0.17626
43	O	−0.18693	0	−0.09698	−0.11492	−0.12263	−0.15344
44	O	−0.15668	0	−0.18734	0.091678	−0.06265	−0.24659
45	C	−0.00073	0	0.046211	−0.00168	−0.0211	−0.12534
46	O	−0.16028	0	0.201714	−0.02545	0.084635	−0.24988
47	C	−0.0021	0	−0.01587	0.002639	−0.04635	−0.12681
48	H	0.0492	0	0.001446	−0.06966	0.12059	0.123958
49	H	0.029195	0	−0.01867	0.05701	−0.10808	0.102601
50	H	0.042061	0	0.037554	0.055156	−0.1093	0.123481
51	H	0.109756	0	0.014851	−0.06915	0.117506	0.337769
52	H	0.043434	0	0.033906	−0.01899	0.134688	0.104385
53	H	0.061391	0	−0.03438	0.005337	−0.15872	0.120544
54	H	0.048	0	0.090244	−0.00055	−0.11691	0.10959
55	H	0.056684	0	−0.02168	0.044736	−0.14725	0.11737
56	H	0.059252	0	0.021474	−0.04257	0.153111	0.118544
57	H	0.047365	0	0.074751	−0.11248	0.056976	0.108208
58	H	0.052212	0	−0.07702	−0.07963	−0.09684	0.117717
59	H	0.068792	0	−0.05938	−0.001	−0.14985	0.133162
60	H	0.067136	0	0.0794	0.101958	0.071643	0.140965
61	H	0.176476	0	−0.14501	−0.00074	0.093179	0.354581
62	H	0.05119	0	0.023337	0.068159	−0.13548	0.108762
63	H	0.063025	0	0.141032	0.006134	−0.08233	0.122198
64	H	0.041463	0	−0.1193	−0.00948	0.070555	0.106123
65	H	0.178404	0	0.019841	−0.0903	0.146117	0.356594
66	H	0.045412	0	−0.07342	−0.09449	−0.07358	0.104131
67	H	0.042111	0	−0.06775	−0.00475	0.114917	0.104866
68	H	0.057655	0	−0.06617	0.13101	−0.05061	0.117771
69	H	0.04367	0	−0.00396	0.104912	−0.08399	0.106741
70	H	0.056756	0	−0.08027	0.068123	0.113081	0.116846

Open Access Article. Published on 19 August 2025. Downloaded on 3/29/2026 11:26:00 PM.
This article is licensed under a Creative Commons Attribution-NonCommercial 3.0 Unported Licence.

Table 6 (*continued*)

Sr no	Atoms	Q–H	S–H	D_x	D_y	D_z	Q-CM5
71	H	0.045905	0	0.134335	0.017385	0.046792	0.104515
72	H	0.062451	0	0.032439	−0.08589	0.129213	0.122995
73	H	0.048821	0	−0.05247	0.117842	0.061751	0.107612
74	H	0.04955	0	−0.11129	−0.07488	−0.05273	0.108353
75	H	0.061146	0	−0.13988	0.003647	0.073015	0.121652
76	H	0.048812	0	0.051977	−0.12357	0.051978	0.107566
77	H	0.049134	0	0.063326	0.101004	0.069737	0.107987

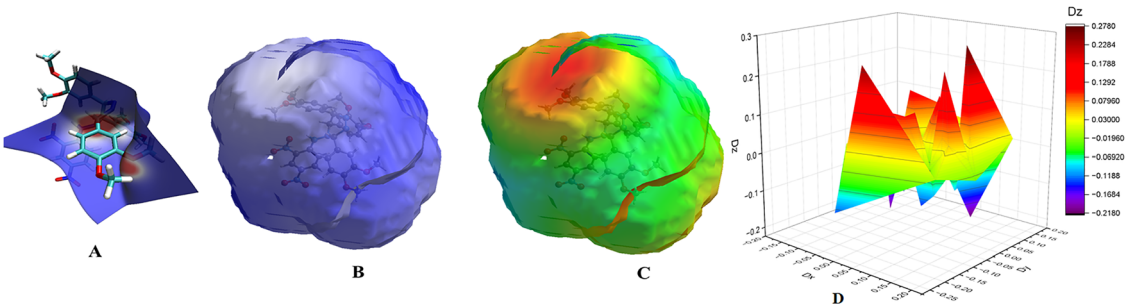

Fig. 14 (A) Molecular structure of **4c** with the surface, showing that their contact is close (red dots represent strong interactions between molecules); (B) Hirshfeld-mapped shape index showing pi–pi stacking interaction using red and blue triangles; (C) Hirshfeld surface and the property of curviness, where flat regions (green) suggest pi–pi stacking and curved (blue) are regions, edges or corners; and (D) surface area graph visualization for dipole components of **4c**.

indicate the electronic environment region of an atom. The LOL/ELF map has a scale in the range of 0.00–1.00.[63] ELF describes the electron pair density, while the LOL describes the maximum number of localized orbitals. This map shows covalent bonding due to the maximum number of electron pairs occupying the space between the molecules. This map scale with a value of <0.5 shows the delocalization of electrons. A high degree of electron localization is indicated by red and orange colors. The blue circle area indicates the inner and valence shells.[64] ELF also enables the quantitative examination of aromaticity in terms of molecular bonding, chemical structure and reactivity. The maximum ELF value is shown by red color, intermediate value shown by yellow to green and minimum value by blue color.[65] The dyeing power of any molecule or compound depends on the extent of conjugation around its azo-linkage, delocalization of π-electrons in a planar system such as phenyl ring (as in our compounds under study **1c–5c** having a 4-phenyl ring system with different substituents) and this delocalization leads to charge transfer between the acceptor and donor groups present around the planar system.

In the current study, all the compounds (**1c–5c**) exhibited aromaticity due to their phenyl ring and lone pairs of electrons, which are present on the methoxy groups, hydroxy, nitro and chloro groups. Thus, the electron pair delocalization of these compounds (**1c–5c**) occupied the blue region with a value of <0.4 and electron localization occupied the red region with a value of >0.7. Therefore, the higher LOL between the azo-linkage and phenyl ring system causes the effective conjugation of the π-electrons, enhances the color intensity and develops a strong dye–fiber interaction. Furthermore, due to the aromatic system and substituted groups, delocalization of charge in the azo-linkage causes a bathochromic shift, which results in the intense color. The substitution of hydroxyl group (–OH) causes an increase in π-conjugation through resonance and electron-donating characteristics. Thus, overall, LOL increases in the aromatic region that enhances the dyeing power of a compound. The substitution of methoxyl groups ($-OCH_3$) behaves similarly to –OH but its effect less than –OH and it causes an increase in LOL around the phenyl ring and azo-linkage due to the electron-donating property of methoxyl ($-OCH_3$). This is why compounds **1c–4c** behave as moderate dyes in comparison to **5c**. The substituted chloro (–Cl) behaves as both electron-withdrawing through the inductive effect and electron-donating through resonance. Its capacity to polarize the electron density stabilizes the azo-linkage and behaves neutrally on the color-imparting strength of the molecule. However, compound **5c** behaves slightly different due to the presence of an additional $-NO_2$ (electron-withdrawing group) because it create a push–pull system that enhances the fabric-dye affinity and intensity of the color developed. The purpose of ELF is to locate the probability of electro pairs in the specific region of a dye molecule, which provides information regarding π/δ-bond localization, intermolecular charge transfer and electron delocalization of chromophores, as observed in the ELF maps (Fig. 15). The delocalization of charge reduces the π-system location across the azo-linkage, leading to an increase in dye strength, *e.g.*, in the ELF map of **1c** (Fig. 15a and b), the presence of a chloro group stabilizes the molecule due to its strong inductive electron-withdrawing influence compared to electron-donating potential. The presence of a methoxy group ($-OCH_3$) opposite the $-NO_2$ group enhances the localization on the nitrogen atom of the azo-linkage, developing

 © 2025 The Author(s). Published by the Royal Society of Chemistry

Open Access Article. Published on 19 August 2025. Downloaded on 3/29/2026 11:26:00 PM.
This article is licensed under a Creative Commons Attribution-NonCommercial 3.0 Unported Licence.

Table 7 Hirshfeld parameters of compound **4c**

Sr no	Atoms	Q–H	S–H	D_x	D_y	D_z	Q-CM5
1	C	0.021321	0	−0.00373	−0.00381	−0.0362	0.025795
2	C	0.030514	0	−0.02149	−0.0223	−0.01445	0.038033
3	N	−0.08391	0	0.162101	−0.03001	0.009116	−0.25677
4	C	0.07278	0	−0.01847	0.048206	0.000705	0.132448
5	C	−0.02441	0	−0.04527	0.047192	−0.00227	−0.03025
6	C	−0.01891	0	0.046027	−0.03538	−0.0041	−0.02527
7	N	−0.06156	0	−0.00922	0.028601	−0.04739	−0.35596
8	C	−0.0646	0	−0.01136	0.028401	0.026705	−0.113
9	C	0.067278	0	0.072248	−0.02523	0.102423	0.086778
10	C	0.064825	0	0.117733	−0.06353	0.015168	0.083783
11	C	−0.06959	0	0.020438	−0.01102	−0.03772	−0.12168
12	C	−0.06032	0	−0.00839	0.010548	−0.04837	−0.1114
13	C	−0.08015	0	0.033209	0.006108	0.007651	−0.12994
14	C	0.062968	0	0.025273	0.120535	0.051638	0.08174
15	C	0.062171	0	−0.07313	0.107765	0.012842	0.081604
16	C	−0.0536	0	−0.04038	−0.0101	−0.03137	−0.10407
17	C	−0.064	0	−0.02533	−0.02788	−0.01606	−0.11514
18	C	0.091769	0	0.038048	0.012513	−0.03279	0.163671
19	C	−0.04407	0	0.009303	0.015778	−0.03238	−0.09007
−0	C	−0.0126	0	−0.06193	0.012285	0.0059	−0.05974
21	C	0.027005	0	−0.07519	−0.02389	0.067485	0.081154
22	C	−0.01938	0	0.017913	−0.0281	0.027846	−0.05665
23	C	0.022821	0	0.087302	−0.01425	−0.02642	0.085722
24	C	−0.01787	0	0.042834	0.043644	0.005633	−0.01892
25	C	−0.06473	0	0.035156	−0.02623	0.017021	−0.11652
26	C	−0.05466	0	0.00579	−0.04531	0.02789	−0.10512
27	C	0.064221	0	−0.10774	−0.0692	−0.02634	0.083749
28	C	0.061663	0	−0.11022	0.030044	−0.06656	0.080514
29	C	−0.07174	0	−0.00653	0.024074	−0.01349	−0.11878
30	N	−0.07001	0	0.112638	0.030306	0.276742	−0.15725
31	N	−0.07181	0	0.006465	−0.18433	0.245803	−0.15991
32	O	−0.14335	0	−0.08237	0.020235	−0.20565	−0.23057
33	C	−0.00166	0	−0.01789	0.013823	0.047779	−0.12661
34	O	−0.14521	0	0.162706	−0.14787	−0.00845	−0.23283
35	C	−0.00249	0	−0.05073	−0.00094	−0.0146	−0.12741
36	O	−0.17502	0	0.11517	−0.05316	0.226053	−0.25574
37	C	−0.01146	0	−0.00067	−0.01272	−0.04658	−0.13586
38	N	0.20635	0	−0.0113	−0.00563	0.011663	0.049386
39	O	−0.20347	0	−0.03524	0.122502	−0.15728	−0.16891
40	O	−0.20504	0	0.195803	−0.05186	−0.02853	−0.17074
41	N	0.202504	0	0.023053	−0.00733	−0.00012	0.04351
42	O	−0.19535	0	−0.16716	0.022425	0.097095	−0.17927
43	O	−0.18779	0	−0.0936	0.110682	−0.13037	−0.15417
44	O	−0.17372	0	0.071884	0.122166	−0.21632	−0.25459
45	C	−0.01124	0	0.01017	−0.0028	0.047776	−0.13564
46	O	−0.14682	0	0.157296	0.153237	0.018347	−0.23453
47	C	−0.00236	0	−0.0008	−0.04959	0.013288	−0.1274
48	O	−0.17635	0	−0.04025	−0.22276	−0.12932	−0.25717
49	C	−0.01286	0	0.00062	0.045458	−0.00337	−0.13784
50	H	0.053449	0	0.040454	0.139322	−0.01053	0.125278
51	H	0.046663	0	0.06193	0.017726	0.117081	0.125693
52	H	0.044946	0	0.097386	−0.07574	−0.00927	0.130364
53	H	0.103641	0	0.11241	−0.01724	−0.03887	0.32766
54	H	0.04964	0	−0.05209	0.054712	0.128438	0.112674
55	H	0.050539	0	0.051354	−0.04235	−0.13946	0.110261
56	H	0.050405	0	−0.03793	0.013977	−0.14264	0.114138
57	H	0.044058	0	0.13723	0.012215	0.050473	0.105048
58	H	0.056556	0	−0.14379	−0.02934	−0.05798	0.116338
59	H	0.039352	0	−0.05268	−0.1024	−0.05292	0.10357
60	H	0.05391	0	−0.07227	0.076494	−0.08454	0.121034
61	H	0.068542	0	−0.14365	0.066997	−0.02991	0.132851
62	H	0.06591	0	0.044493	−0.09131	0.107292	0.139513
63	H	0.043763	0	0.116952	−0.06021	0.060532	0.103495
64	H	0.058351	0	0.020046	−0.14837	0.057502	0.118165
65	H	0.044826	0	−0.01583	0.12659	−0.04933	0.111686
66	H	0.062165	0	0.136517	−0.06486	0.046496	0.122827
67	H	0.047746	0	−0.05417	−0.10705	−0.07753	0.106342
68	H	0.048893	0	0.049432	0.097816	−0.09252	0.107631
69	H	0.046846	0	0.052169	−0.06731	0.113823	0.105388
70	H	0.048371	0	0.104937	0.006445	−0.09676	0.107106

Open Access Article. Published on 19 August 2025. Downloaded on 3/29/2026 11:26:00 PM.
This article is licensed under a Creative Commons Attribution-NonCommercial 3.0 Unported Licence.

Table 7 (*continued*)

Sr no	Atoms	Q–H	S–H	D_x	D_y	D_z	Q-CM5
71	H	0.061685	0	0.00362	0.148957	0.05182	0.122336
72	H	0.038568	0	0.060603	0.101626	0.063791	0.103645
73	H	0.05432	0	−0.12157	0.089575	−0.02388	0.114669
74	H	0.040839	0	−0.04255	−0.07776	0.106438	0.099584
75	H	0.04099	0	0.083522	−0.03969	−0.10319	0.099801
76	H	0.053992	0	−0.09363	−0.1199	0.012936	0.114377
77	H	0.038793	0	−0.09747	0.06621	−0.06612	0.104058
78	H	0.060366	0	−0.14066	0.011147	−0.0681	0.120995
79	H	0.047538	0	−0.01112	0.105114	0.092203	0.106324
80	H	0.05023	0	0.084883	0.047345	−0.10758	0.108936
81	H	0.054269	0	0.056082	0.015835	0.141784	0.114647
82	H	0.035904	0	−0.06482	−0.08339	0.018266	0.098647
83	H	0.037707	0	0.096954	−0.08508	−0.03086	0.102568

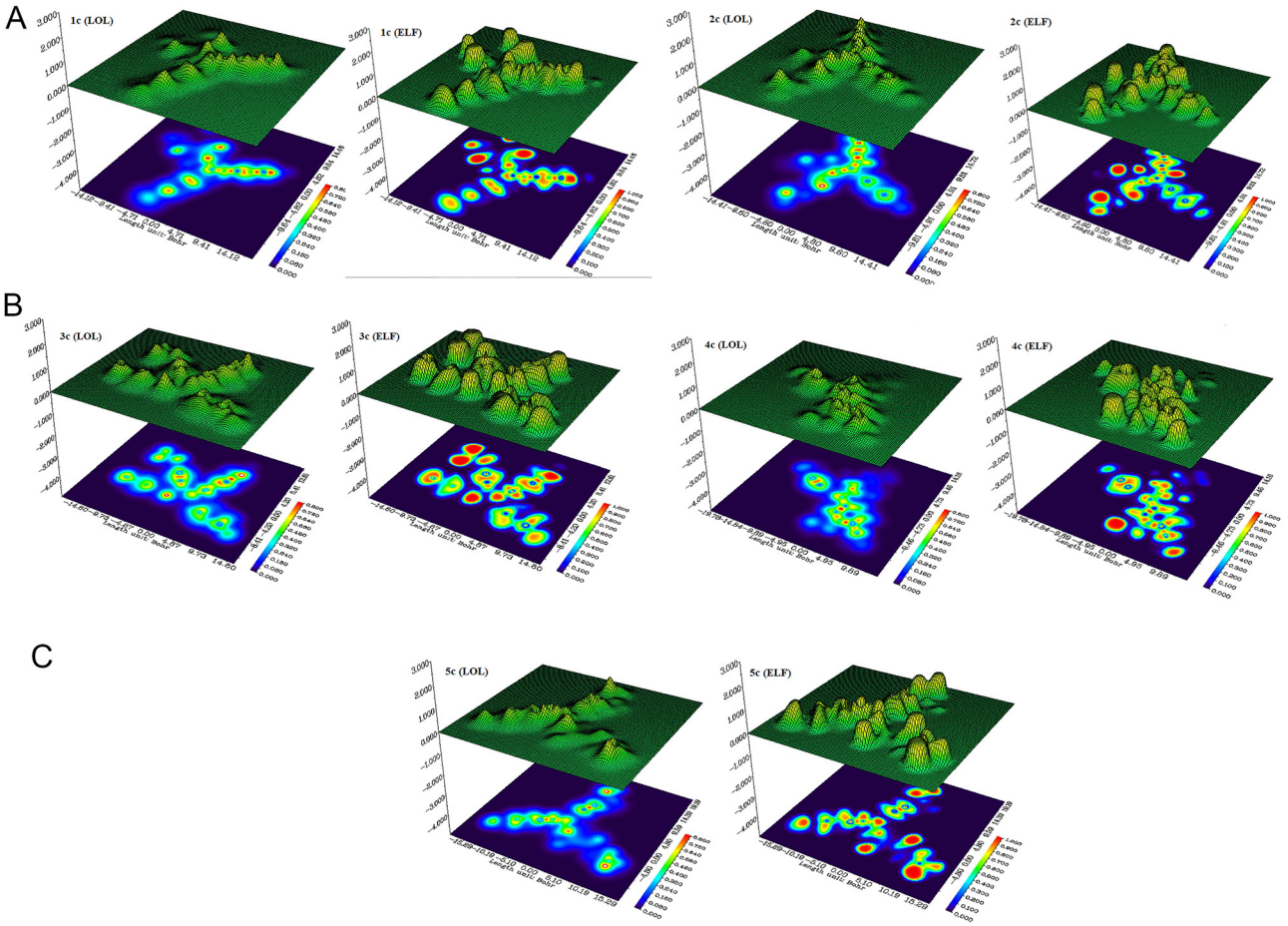

Fig. 15 (a) Localized orbital locator (LOL) and electron localization function (ELF) projection maps of compounds **1c** and **2c**. (b) Localized orbital locator (LOL) and electron localization function (ELF) projection maps of compounds **3c** and **4c**. (c) Localized orbital locator (LOL) and electron localization function (ELF) projection maps of compound **5c**.

an intense color but reduced fastness in the case of **5c**. Similarly, in **2c**–**4c**, the hydroxyl (–OH) and methoxyl (–OCH_3) groups affect the ELF and cause delocalization, which results in resonance stabilization, enhancing the dye strength.

3.5.4.2. NCI and RDG analysis. The reduced density gradient (RDG) analysis was introduced by Jonson and colleagues, which is based on non-covalent interactions (NCI) and provides a topological tool for viewing these interactions in a molecule. In the structure of a molecule with different types of interactions such as attractive and repulsive forces, they can be identified by plotting RDG and NCI maps against electron density ($\sin(\lambda 2)\rho$). This analysis was performed using the Multiwfn and VMD programs.[66] This analysis provides knowledge about van der

 © 2025 The Author(s). Published by the Royal Society of Chemistry

Open Access Article. Published on 19 August 2025. Downloaded on 3/29/2026 11:26:00 PM.
This article is licensed under a Creative Commons Attribution-NonCommercial 3.0 Unported Licence.

Waals interactions, H-bonding and steric repulsion in molecular complexes and small molecules. In the plot, red color describes strong repulsion, green color describes van der Waals interaction and blue color describes strong H-bonding interactions.[63]

All the compounds (**1c**–**5c**) exhibited strong repulsive forces in their phenyl ring, van der Waals forces in the region of their methoxy and nitro groups, and hydrogen bonding with the nitrogen adjacent to their central core towards the hydrogen of their phenyl ring, as shown in Fig. 16. The presence of an –OH group in compounds **1c** and **3c** developed strong intermolecular hydrogen bonding between the dye and fabric, which increased the dye fixation on the fibers, resulting in the strong dyeing capacity of these molecules. Electron-withdrawing groups such as $-NO_2$ and –Cl also enhance the dye–fiber interaction and intense color development but the colour fastness is reduced due the –Cl polarizability property and the π–π stacking caused by $-NO_2$.

This is the reason why the presence of electron-donating groups such as –OH and $-OCH_3$ raises the HOMO energy level and electron-withdrawing groups such as $-NO_2$ and –Cl raises the LUMO energy level, which influence the color intensity in a broader way. Moreover, NCI studies also explain the effect of substituents on the azo-dye interaction with fabric. In the maps (Fig. 16), it can be seen that the electron-donating groups present in the blue/green region increase the intermolecular hydrogen bonding, which enhances the dye–fiber interaction, resulting in better fixation. In contrast, the chloro group is in the red region because of the steric repulsion, resulting in reduced dye strength. The $-NO_2$ group attached to aromatic ring causes an enhancement in π–π stacking with textile fibers, leading to an increment in the strength and intensity of color on textiles, as in the case of **5c**.

Conclusion

In this research, we reported the cycloaddition reactions of azodiene and azodienophile to synthesize azo dyes of 1,2,4-triazine derivatives (**1c**–**5c**). The dyeing abilities of these five azo dyes were explored in terms of colorfastness tests on polyester fabric. All dyes showed excellent results in the colorfastness assessments. However, in the case of colorfastness to light, four dyes, **1c**–**4c**, revealed poor results for light absorption under a xenon arc lamp, whereas one dye, **5c**, revealed average results. This can be attributed to the fact that **5c** has one additional electron-withdrawing group, *i.e.* nitrobenzene attached to the triazine core, than the others. If an electron-withdrawing group is present in one ring and electron-donating group on another aromatic ring, they increase the absorption intensity, color strength and polarity of the azo bond. All the dyes were evaluated for their *in vitro* antibacterial activities through the agar disc diffusion method with good results using *E. coli* and *Staphylococcus aureus* strains. The solvatochromism of these dyes in solvents with different polarity was checked based on their λ_{max} values. The experimental results for all the dyes showed that they have almost the same λ_{max} values as that from TD-SCF DFT calculations on different polarity. However, the photochromism of all the dyes in different polarity solvents showed a change in color under UV-light and normal sunlight. Additionally, all the dyes showed better results of molecular docking against bacteria. The Hirshfeld analysis also supported the dyeing capacity of the molecules in terms of experimental results by displaying the hydrogen bonding tendency of molecules **1c**–**5c** for strong intermolecular hydrogen bonding. Moreover, the topological studies, *i.e.* LOL, ELF, NCI and RDG, predicted the localized and delocalized regions of electrons and non-covalent interactions such as van der Waals, hydrogen

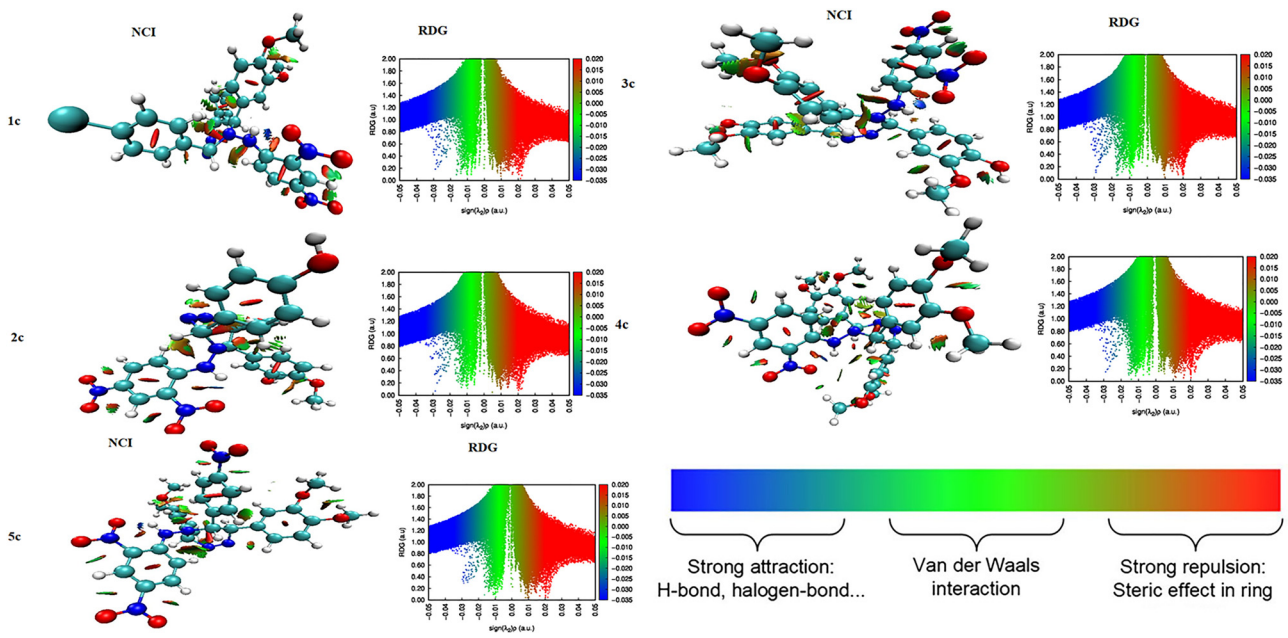

Fig. 16 RDG scatter analysis and NCI analysis of target compounds **1c**–**5c**.

Open Access Article. Published on 19 August 2025. Downloaded on 3/29/2026 11:26:00 PM.
This article is licensed under a Creative Commons Attribution-NonCommercial 3.0 Unported Licence.

bonding and steric repulsions within the compounds (**1c–5c**). Alternatively, DFT analysis of compounds **1c–5c** confirmed their favorable electronic structures and chemical reactivity, supporting their potential as stable and effective candidates for advanced functional applications in materials and biological sciences.

Author contributions

Saima Aslam conduct the compound synthesis and analysis, molecular docking study, original paper writing; Basharat Ali concieved the conceptualization of study and supervision of study; Nusrat Shafiq* manage all sources, software and drafting and write up of original paper; Shahzad Murtaza works on proof reading, editing and English check.

Conflicts of interest

Authors have no conflict of interest.

Data availbility

Supplementary information is available. See DOI: **https://doi.org/10.1039/d5ma00587f**

Data will be available upon request. All the authors confirm that the data which supporting the findings of this study are available within the article as its SI. The supplementary information provides Fig. S1, Fig. S2, Fig. S3, Fig. S4, Fig. S5, Fig. S6, Fig. S7. Table S1.

Acknowledgements

Authors thankful to Synthetic and Natural Products Discovery Laboratory Government College Women University Faisalabad-Pakistan to provide facility of Synthesis and antibacterial evaluation.

References

1 A. Panitsiri, S. Tongkhan, W. Radchatawedchakoon and U. Sakee, *J. Mol. Struct.*, 2016, **1107**, 14–18.
2 M. N. Bukhari, M. Shabbir, L. J. Rather, M. Shahid, U. Singh, M. A. Khan and F. Mohammad, *Text. Clothing Sustainability*, 2017, **3**, 1–9.
3 R. Sahilu, R. Eswaramoorthy, E. Mulugeta and A. Dekebo, *J. Mol. Struct.*, 2022, **1265**, 133279.
4 S. Benkhaya, S. M'rabet and A. E. Harfi, *Heliyon*, 2020, **6**, e03271.
5 J.-S. Bae, K. S. Kim, J. H. Park and S. D. Kim, *Dyes Pigm.*, 2007, **75**, 170–175.
6 S. Samsami, M. Mohamadizaniani, M.-H. Sarrafzadeh, E. R. Rene and M. Firoozbahr, *Process Saf. Environ. Prot.*, 2020, **143**, 138–163.
7 S. Benkhaya, S. M'rabet and A. El Harfi, *Heliyon*, 2020, **6**, 1–26.
8 S. El Harfi and A. El Harfi, *Appl. J. Environ. Eng. Sci.*, 2017, **3**, 311–320.
9 Y. D. Aracagök and N. Cihangir, *Am. J. Microbiol. Res.*, 2013, **1**, 16–20.
10 R. W. Sabnis, *Color. Technol.*, 2016, **132**, 49–82.
11 E. El-Sayed, E. A. El-Aziz, H. Othman and A. G. Hassabo, *Egypt. J. Chem.*, 2024, **67**, 87–97.
12 U. H. Siddiqua, S. Ali, M. Iqbal and T. Hussain, *J. Mol. Liq.*, 2017, **241**, 839–844.
13 W. H. Mahmoud, F. N. Sayed and G. G. Mohamed, *Appl. Organomet. Chem.*, 2016, **30**, 959–973.
14 C. Kantar, H. Akal, B. Kaya, F. Islamoğlu, M. Türk and S. Şaş maz, *J. Organomet. Chem.*, 2015, **783**, 28–39.
15 Z. Ghasemi, S. Azizi, R. Salehi and H. S. Kafil, *Monatsh. Chem.*, 2018, **149**, 149–157.
16 M. A. Gouda, H. F. Eldien, M. M. Girges and M. A. Berghot, *J. Saudi Chem. Soc.*, 2016, **20**, 151–157.
17 A. M. Saeed, S. S. AlNeyadi and I. M. Abdou, *Heterocycl. Commun.*, 2020, **26**, 192–205.
18 B. K. Ho, Z. Ngaini, P. Matthew Neilsen, S. S. Hwang, R. Entigu Linton, E. L. Kong and B. K. Lee, *J. Chem.*, 2017, **2017**, 6760413.
19 F. A. Saad, H. A. El-Ghamry, M. A. Kassem and A. M. Khedr, *J. Inorg. Organomet. Polym. Mater.*, 2019, **29**, 1337–1348.
20 M. A. Muhammad-Ali, H. H. Salman and E. Jasim, *Asian J. Pharm. Clin. Res.*, 2019, **12**, 479–483.
21 D. A. Kennedy, N. Vembu, F. R. Fronczek and M. Devocelle, *J. Org. Chem.*, 2011, **76**, 9641–9647.
22 S. Harisha, J. Keshavayya, S. Prasanna and H. J. Hoskeri, *J. Mol. Struct.*, 2020, **1218**, 128477.
23 H. A. Hekal, R. M. Kassab, H. A. A. E. Salam, E. Shaban and F. M. Atlam, *ChemistrySelect*, 2023, **8**, e202204075.
24 M. A. Sakr and M. T. A. Kana, *J. Fluoresc.*, 2022, **32**, 2053–2063.
25 A. Arkak, M. H. Sadr, M. Janghouri, F. Marandi and D. Fuhrmann, *RSC Adv.*, 2024, **14**, 22006–22016.
26 H. F. Rizk, S. A. Ibrahim and M. A. El-Borai, *Arabian J. Chem.*, 2017, **10**, S3303–S3309.
27 F. Bibi, I. Ahmad, S. Hussain and M. Ibrahim, *Ceram. Int.*, 2024, **50**, 53319–53328.
28 U. Arshad and S. Ahmed, 2021, **vol. 26**.
29 M. Khalid, M. U. Khan, N. Azhar, M. N. Arshad, A. M. Asiri, A. A. C. Braga and M. N. Akhtar, *Opt. Quantum Electron.*, 2022, **54**, 395.
30 M. Maqsood, N. Shafiq and M. T. Hussain, *J. Mol. Struct.*, 2025, **1321**, 140096.
31 D. R. Waring and G. Hallas, *The chemistry and application of dyes*, Springer Science & Business Media, 2013.
32 D. Maliszewski and D. Drozdowska, *Pharmaceuticals*, 2022, **15**, 1–19.
33 P. Singla, V. Luxami and K. Paul, *Eur. J. Med. Chem.*, 2015, **102**, 39–57.
34 H. Guo and Q. P. Diao, *Curr. Top. Med. Chem.*, 2020, **20**, 1481–1492.
35 S. Singh, M. K. Mandal, A. Masih, A. Saha, S. K. Ghosh, H. R. Bhat and U. P. Singh, *Arch. Pharm.*, 2021, **354**, e2000363.

 © 2025 The Author(s). Published by the Royal Society of Chemistry

Open Access Article. Published on 19 August 2025. Downloaded on 3/29/2026 11:26:00 PM.
This article is licensed under a Creative Commons Attribution-NonCommercial 3.0 Unported Licence.

36 H. Liu, S. Long, K. Rakesh and G.-F. Zha, *Eur. J. Med. Chem.*, 2020, **185**, 111804.
37 N. Madu, E. C. Ikechukwu, C. N. Anyao, I. E. Mbakwe, K. N. Maduako, M. I. Okereke and J. N. Madu, *Int. Res. Mater. Environ.*, 2024, **4**, 12–20.
38 T. V. Parmar and H. H. Desai, *Chem. Biol. Interface*, 2021, **11**(3), 116–123.
39 A. Negi, *Polymers*, 2025, **17**, 871.
40 N. Salih, J. Salimon and H. Hussien, *Hemoglobin*, 2021, **18**, 21.
41 F. Duan, G. Xin, H. Niu and W. Huang, *Sci. Rep.*, 2017, **7**, 12721.
42 M. Ghasemian, A. Kakanejadifard, F. Azarbani, A. Zabardasti and S. Kakanejadifard, *J. Mol. Liq.*, 2014, **195**, 35–39.
43 M. A. Rauf and S. Hisaindee, *J. Mol. Struct.*, 2013, **1042**, 45–56.
44 J.-W. Yang, J.-K. Choi, M.-C. Kim and H. Kim, *Prog. Org. Coat.*, 2019, **135**, 168–175.
45 A. Bourbour Hosseinbakhi, A. Mirabi, M. Reza Zardoost, H. Zhao and A. Farajtabar, *J. Mol. Liq.*, 2024, **404**, 124948.
46 M. Sakr and M. Aboukana, *J. Fluoresc.*, 2022, **32**, 3.
47 M. U. Khan, M. Khalid, S. Asim, Momina, R. Hussain, K. Mahmood, J. Iqbal, M. N. Akhtar, A. Hussain and M. Imran, *Front. Mater.*, 2021, **8**, 719971.
48 V. S. Padalkar, V. S. Patil and N. Sekar, *Chem. Cent. J.*, 2011, **5**, 77.
49 E. V. Nosova, G. N. Lipunova, G. V. Zyryanov, V. N. Charushin and O. N. Chupakhin, *Org. Chem. Front.*, 2022, **9**, 6646–6683.
50 C. Zhao, Z. Li, X. Wu, H. Su, F.-Q. Bai, X. Ran, L. Yang, W. Fang and X. Yang, *Small*, 2024, **20**, 2400541.
51 V. Patil, A. Noonikara-Poyil, S. D. Joshi, S. A. Patil, S. A. Patil, A. M. Lewis and A. Bugarin, *J. Mol. Struct.*, 2020, **1220**, 128687.
52 M. Anjomshoa, M. Sahihi, S. J. Fatemi, S. Shayegan, A. Farsinejad and B. Amirheidari, *Biometals*, 2022, **35**, 549–572.
53 R. A. Mekheimer, G. E.-D. A. Abuo-Rahma, M. Abd-Elmonem, R. Yahia, M. Hisham, A. M. Hayallah, S. M. Mostafa, F. A. Abo-Elsoud and K. U. Sadek, *J. Mol. Struct.*, 2022, **1267**, 133615.
54 U. P. Singh, M. Pathak, V. Dubey, H. R. Bhat, P. Gahtori and R. K. Singh, *Chem. Biol. Drug Des.*, 2012, **80**, 572–583.
55 A. A. M. El-Reedy and N. K. Soliman, *Sci. Rep.*, 2020, **10**(1), 1–18.
56 A. Zahirović, S. Fetahović, M. Feizi-Dehnayebi, A. Višnjevac, R. Bešta-Gajević, A. Kozarić, L. Martić, A. Topčagić and S. Roca, *Spectrochim. Acta, Part A*, 2024, 124528.
57 B. Parveen, S. Shahzadi, S. Ali, M. Feizi-Dehnayebi, K. S. Munawar, M. Ashfaq and M. N. Tahir, *J. Mol. Struct.*, 2024, **1315**, 138851.
58 N. Shafiq, A. Mehroze, W. Sarwar, U. Arshad, S. Parveen, M. Rashid, A. Farooq, N. Rafiq, G. F. Wondmie and Y. A. Bin Jardan, *Front. Chem.*, 2023, **11**, 1251529.
59 M. Miar, A. Shiroudi, K. Pourshamsian, A. R. Oliaey and F. Hatamjafar, *J. Chem. Res.*, 2020, **45**, 147–158.
60 M. Dinleyici, B. Al-Khateeb, A. Abourajab, D. Uzun, S. Koyuncu and H. Icil, *J. Photochem. Photobiol., A*, 2021, **421**, 113525.
61 M. Khalid, A. Ali, Z. U. Din, M. N. Tahir, S. F. de Alcantara Morais, A. A. C. Braga, M. N. Akhtar, M. Imran and E. Rodrigues-Filho, *J. Mol. Struct.*, 2021, **1241**, 130650.
62 G. Zarren, N. Shafiq, U. Arshad, N. Rafiq, S. Parveen and Z. Ahmad, *J. Mol. Struct.*, 2021, **122**, 1–14.
63 F. Akman, A. Demirpolat, A. S. Kazachenko, A. S. Kazachenko, N. Issaoui and O. Al-Dossary, *Molecules*, 2023, **28**, 2684.
64 A. Jumabaev, S.-J. Koyambo-Konzapa, H. Hushvaktov, A. Absanov, B. Khudaykulov, U. Holikulov, Z. Ernazarov, N. Issaoui, O. M. Al-Dossary and M. Nsangou, *J. Mol. Model.*, 2024, **30**, 349.
65 N. Azum, M. N. Arshad, M. A. Rub, M. Asad, K. A. Alzahrani and H. M. Marwani, *Adv. Life Sci.*, 2025, **12**, 175–184.
66 J. Sampathkumar and R. Rajamanickam, *J. Mol. Struct.*, 2024, **1299**, 137063.